

Spitzer SAGE Infrared Photometry of Massive Stars in the Large Magellanic Cloud

A. Z. Bonanos^{1,2}, D. L. Massa², M. Sewilo², D. J. Lennon², N. Panagia^{2,3}, L. J. Smith²,
M. Meixner², B. L. Babler⁴, S. Bracker⁴, M. R. Meade⁴, K. D. Gordon², J. L. Hora⁵,
R. Indebetouw⁶, B. A. Whitney⁷

ABSTRACT

We present a catalog of 1750 massive stars in the Large Magellanic Cloud, with accurate spectral types compiled from the literature, and a photometric catalog for a subset of 1268 of these stars, with the goal of exploring their infrared properties. The photometric catalog consists of stars with infrared counterparts in the *Spitzer* SAGE survey database, for which we present uniform photometry from 0.3 – 24 μm in the *UBVIJHK_s*+IRAC+MIPS24 bands. The resulting infrared color–magnitude diagrams illustrate that the supergiant B[e], red supergiant and luminous blue variable (LBV) stars are among the brightest infrared point sources in the Large Magellanic Cloud, due to their intrinsic brightness, and at longer wavelengths, due to dust. We detect infrared excesses due to free–free emission among ~ 900 OB stars, which correlate with luminosity class. We confirm the presence of dust around 10 supergiant B[e] stars, finding the shape of their spectral energy distributions (SEDs) to be very similar, in contrast to

¹Giacconi Fellow.

²Space Telescope Science Institute, 3700 San Martin Drive, Baltimore, MD, 21218, USA; bonanos, massa, sewilo, lennon, panagia, lsmith, meixner, kgordon@stsci.edu

³INAF/Osservatorio Astrofisico di Catania, Via S.Sofia 78, I-95123 Catania, Italy; and Supernova Ltd., VGV #131, Northsound Road, Virgin Gorda, British Virgin Islands.

⁴Department of Astronomy, 475 North Charter St., University of Wisconsin, Madison, WI 53706, USA; brian@sal.wisc.edu, s_bracker@hotmail.com, meade@sal.wisc.edu

⁵Harvard-Smithsonian Center for Astrophysics, 60 Garden St., MS 67, Cambridge, MA 02138, USA; jhora@cfa.harvard.edu

⁶Department of Astronomy, University of Virginia, PO Box 3818, Charlottesville, VA 22903, USA; remy@virginia.edu

⁷Space Science Institute, 4750 Walnut St., Suite 205, Boulder, CO 80301, USA; bwhitney@spacescience.org

the variety of SED shapes among the spectrally variable LBVs. The similar luminosities of B[e] supergiants ($\log L/L_\odot \geq 4$) and the rare, dusty progenitors of the new class of optical transients (e.g. SN 2008S and NGC 300 OT), plus the fact that dust is present in both types of objects, suggests a common origin for them. We find the infrared colors for Wolf-Rayet stars to be independent of spectral type and their SEDs to be flatter than what models predict. The results of this study provide the first comprehensive roadmap for interpreting luminous, massive, resolved stellar populations in nearby galaxies at infrared wavelengths.

Subject headings: infrared: stars– stars: early-type– stars: Wolf-Rayet– stars: emission-line, Be– galaxies: individual (LMC)– catalogs

1. Introduction

The *Spitzer Space Telescope* Legacy Survey called “Surveying the Agents of a Galaxy’s Evolution” (SAGE; Meixner et al. 2006) provides an unprecedented opportunity to investigate the infrared properties of a large number of massive stars ($\gtrsim 8 M_\odot^1$) in the Large Magellanic Cloud (LMC). The SAGE infrared point source catalog has so far enabled studies of evolved stars (Blum et al. 2006; Hora et al. 2008; Srinivasan et al. 2009), young stellar objects (Whitney et al. 2008), and variables (Vijh et al. 2009); however, the hot massive star population remains unexplored. The radiation from hot massive stars at the mid-infrared wavelengths probed by the IRAC (3.6, 4.5, 5.8, 8.0 μm ; Fazio et al. 2004) and MIPS (24, 70, and 160 μm ; Rieke et al. 2004) cameras onboard *Spitzer* consists of: thermal blackbody emission modified by the atmospheric opacity, bound–free and free–free emission (“Bremsstrahlung”), which depend on the density and velocity structure of the stellar wind, and excess emission if circumstellar dust (or a cool companion) exists.

Panagia & Felli (1975) and Wright & Barlow (1975) were the first to calculate the infrared and radio free–free emission from ionized envelopes around hot massive stars, as a function of the mass-loss rate (\dot{M}), terminal velocity (v_∞) of the wind and temperature (T) for the cases of optically thin and thick winds to explain the radio emission from hot stars undergoing mass-loss. They found that the flux as a function of frequency (ν) and distance (d) for an optically thick, spherically symmetric wind at infrared and radio wavelengths scales as: $F_{\nu,thick} \propto \dot{M}^{4/3} v_\infty^{-4/3} \nu^{0.6} d^{-2} T^{0.1}$, while for an optically thin wind: $F_{\nu,thin} \propto \dot{M}^2 v_o^{-2} R^{-1} T^{-1.35} \nu^{-2.1} B_\nu$, where R is the photospheric radius, v_o the initial wind

¹These stars are massive enough to fuse iron in their cores; they end their lives as core-collapse supernovae.

velocity at the surface of the star, and B_ν is the Planck function. These calculations, following the shell model of Gehrz et al. (1974), motivated further infrared and radio observations of Galactic OB stars. The initial studies produced controversial measurements of infrared excesses (see Sneden et al. 1978; Castor & Simon 1983; Abbott et al. 1984), whereas unambiguous excesses were detected in the radio (e.g. Abbott et al. 1981). Leitherer & Wolf (1984) detected infrared excesses in a large number of early-type stars and attributed the previous non-detections to their different treatment of intrinsic stellar colors and interstellar reddening. Bertout et al. (1985) determined the velocity law for this large sample, pointing out that excesses can only be measured reliably in cases of suitably slow (low v_∞) and/or dense (high \dot{M}) winds. In principle, mass-loss rates can be determined from radio observations, which probe the optically thick wind, e.g. as done for OB-type stars (Abbott et al. 1981) and Wolf-Rayet stars (Barlow et al. 1981; Abbott et al. 1986). However, Moffat & Robert (1994) presented observational evidence for clumping in stellar winds, which yields mass-loss rates that are too high when unaccounted for. While clumping, when not accounted for, can undoubtedly lead to an overestimation of the mass loss, the radio observations seem to be least affected by this problem (see e.g., Puls et al. 2006), possibly because the wind is less clumped at larger distances from the star. On the other hand, it has been shown that in many cases a substantial fraction of the radio flux from early-type stars is of non-thermal origin (Abbott et al. 1984; De Becker 2007), thus complicating the interpretation of radio observations.

Until now, work on infrared excesses in hot stars has been limited by (i) the accuracy of ground based observations at wavelengths greater than $5 \mu\text{m}$, where infrared excess due to free-free or dust emission becomes significant, and (ii) the systematic errors associated with disentangling reddening and distances for Galactic stars, which can be substantial. The advent of *Spitzer*, therefore, provides an opportunity to readdress and quantify the infrared excesses in hot massive stars at half-solar metallicity. For the first time, a large number of stars in the LMC have been observed uniformly out to $24 \mu\text{m}$. The low foreground reddening of this sample of stars, located at the same distance, circumvents the problems encountered with extincted Galactic early-type stars, which are observed against a bright infrared background and distributed at various distances throughout the Galactic plane. With the goal of characterizing their infrared properties, we have compiled a catalog of luminous massive stars with known spectral types in the LMC and extracted infrared photometry for these stars from the SAGE database. Our results not only serve as a valuable starting point for more detailed work on specific types of massive stars, but also provide a roadmap for interpreting existing and future infrared observations of the most luminous stars in nearby galaxies.

Besides the LMC, *Spitzer* has imaged the following Local Group galaxies: the SMC (Bolatto et al. 2007), M31 (Mould et al. 2008), M33 (Verley et al. 2007; McQuinn et al.

2007; Thompson et al. 2008), WLM (Jackson et al. 2007a), IC 1613 (Jackson et al. 2007b), NGC 6822 (Cannon et al. 2006), and the dwarf irregulars: Phoenix, LGS 3, DDO 210, Leo A, Pegasus, and Sextans A (Boyer et al. 2009). Only a small fraction of the massive stars in these galaxies have spectroscopic classifications, rendering identifications of objects based on their infrared colors uncertain. Our results, which are based on stars with accurate spectral classifications, will help interpret these photometric observations. An advantage of studying stars in the LMC, rather than in more distant Local Group galaxies, is that blending problems are minimized. For example, the angular resolution at the IRAC 3.6 μm band is 1."7, which corresponds to 0.4 pc in the LMC (at a distance of 48.1 kpc; Macri et al. 2006), and 8 pc in M33 (at a distance of 964 kpc; Bonanos et al. 2006), while typical OB associations have sizes of tens of parsecs (but half light radii of several parsecs), and young massive clusters can have sizes smaller than a parsec (Clark et al. 2005).

The paper is organized as follows: §2 describes our spectroscopic and photometric catalogs of massive stars in the LMC, §3 presents the resulting color–magnitude diagrams, §4 the two–color diagrams, and §5 the infrared excesses detected in OB stars. Sections §6, §7, §8, §9 describe the infrared properties of Wolf-Rayet stars, luminous blue variables, supergiant B[e] stars, and red supergiants, respectively, and §10 summarizes our results.

2. Catalog of Massive Stars in the LMC

We first compiled a catalog of massive stars with known spectral types in the LMC from the literature. We then cross-matched the stars in the SAGE database, after incorporating optical and near-infrared photometry from recent surveys of the LMC. The resulting photometric catalog was used to study the infrared properties of the stars. In §2.1 we describe the spectral type catalog compiled from the literature, in §2.2 the existing optical, near-infrared and mid-infrared surveys of the LMC that were included in the SAGE database, and in §2.3 the cross-matching procedure and the resulting photometric catalog.

2.1. Spectral Type Catalog

The largest existing catalogs of OB stars in the LMC were compiled by Sanduleak (1970, 1273 stars) and Rousseau et al. (1978, 1822 stars); however the accuracies of the coordinates (arcminute precision) and spectral types (from objective prism spectra) are not sufficient for a comparison with the SAGE database. Despite the monumental effort of Brian Skiff to update coordinates of these stars by manually identifying each one from the original findercharts (see

Sanduleak 2008), improved spectral types require new spectroscopy and acquiring them is an even more difficult task. We therefore compiled a new catalog of massive stars from the literature, by targeting OB stars having both accurate coordinates and spectral classifications, making some of these available for the first time in electronic format. The literature search resulted in 1750 entries. We do not claim completeness; however, we have targeted studies of hot massive stars (defined by their spectral types) in individual clusters and OB associations, as well as studies of particular types of massive stars. The largest studies included are: Conti et al. (1986, new spectral types for 191 OB stars), Fitzpatrick (1988, 1991, study of supergiants²), Massey et al. (1995, new spectral types for 179 OB stars), Massey et al. (2000, study of 19 OB associations), the VLT-FLAMES survey (Evans et al. 2006, 238 stars in N11 and NGC 2004), the studies of the 30 Doradus region by Schild & Testor (1992), Parker (1993) and Walborn & Blades (1997), and the Wolf-Rayet catalog from Breysacher et al. (1999). Note, we have omitted stars from the crowded R136 cluster. We have added the 6 known luminous blue variables (Humphreys & Davidson 1994), 10 supergiant B[e] stars (Zickgraf 2006), 20 Be/X-ray binaries (Liu et al. 2005; Raguzova & Popov 2005) and early-type eclipsing and spectroscopic binaries. For comparison, we also included 147 red supergiants from Massey & Olsen (2003), some of which were originally classified by Humphreys (1979). The completeness of the catalog depends on the spectral type, e.g. it is $\sim 3\%$ for the unevolved O stars in our catalog (out of an estimated total of 6100 unevolved stars with masses $> 20 M_{\odot}$ in the LMC; Massey 2009), while the Wolf-Rayet catalog (Breysacher et al. 1999) is thought to be close to complete.

Table 1 presents our catalog of 1750 massive stars, listing: the star name, coordinates in degrees (J2000.0), the reference and corresponding spectral classification, along with comments. The names of the stars are taken from the corresponding reference and are sorted by right ascension. The spectral classifications in the catalog are typically accurate to one spectral type and one luminosity class. We retained about a dozen stars from the above studies with only approximate spectral types (e.g. “early B”). For double entries, we included the best spectral classification available, usually corresponding to the most recent reference. We updated coordinates for all stars with names from the Sanduleak, Brunet, and Parker catalogs from Brian Skiff’s lists³. Our catalog contains 427 stars from the Sanduleak catalog, 81 from the Brunet catalog and 148 from the Parker catalog.

²We have corrected the typographical error in the name of the B7 Ia+ star Sk -67° 143 given by Fitzpatrick (1991) to the correct name: Sk -69° 143.

³<ftp://ftp.lowell.edu/pub/bas/starcats/>

2.2. Optical and Infrared Surveys of the LMC

Several large optical and infrared photometric catalogs of the LMC have recently become available, enabling us to obtain accurate photometry for its massive star population in the wavelength region $0.3 - 8 \mu\text{m}$ and in some cases up to $24 \mu\text{m}$. The optical surveys are: the *UBVR* catalog of Massey (2002) with 180,000 bright stars in an area covering 14.5 square degrees, the *UBVI* Magellanic Clouds Photometric Survey (MCPS; Zaritsky et al. 2004) including 24 million stars in the central 64 square degrees, and the OGLE III catalog containing *VI* photometry of 35 million stars covering 40 square degrees (Udalski et al. 2008). The angular resolution for each survey is $\sim 2.''6$ for the catalog of Massey (2002), $\sim 1.''5$ for MCPS, and $\sim 1.''2$ for OGLE III.

The existing near-infrared photometric catalogs include: the Two Micron All Sky Survey (2MASS; Skrutskie et al. 2006, extended by 6X2MASS) and the targeted IRSF survey (Kato et al. 2007), which contains 14.8 million sources in the central 40 square degrees of the LMC. 2MASS has a pixel scale of $2.''0 \times 2.''0$, an average seeing of $2.''5$ and limiting magnitudes of $J = 15.8$, $H = 15.1$ and $K_s = 14.3$. IRSF has a pixel scale of $0.''45 \text{ pixel}^{-1}$, average seeing of $1.''3$, $1.''2$, $1.''1$ in the *JHK_s* bands, respectively, and limiting magnitudes of $J = 18.8$, $H = 17.8$ and $K_s = 16.6$. In the mid-infrared, the *Spitzer* SAGE survey uniformly imaged the central $7^\circ \times 7^\circ$ of the LMC in the IRAC and MIPS bands on two epochs in 2005, separated by 3 months (Meixner et al. 2006). The survey has recently produced a combined mosaic catalog of 6.4 million sources. IRAC, with a pixel scale of $1.''2 \text{ pixel}^{-1}$, yields an angular resolution of $1.''7 - 2.''0$ and MIPS at $24 \mu\text{m}$ has a resolution of $6''$.

Given the variation in the depth, resolution and spatial coverage of these surveys, we included the available photometry for the massive stars in our catalog from all the MCPS, OGLE III, 2MASS, IRSF and SAGE catalogs. MCPS has incorporated the catalog of Massey (2002) for bright stars common to both catalogs. We note that due to problems with zero-point, calibration and PSF fitting of bright stars, MCPS photometry of bright stars should be used with caution. The authors warn that stars “brighter than 13.5 mag in *B* or *V* are prone to substantial photometric uncertainty” (Zaritsky et al. 2004). Photometry of higher accuracy, particularly in the optical, exists in the literature for many of the stars in our catalog; however, it was not included in favor of uniformity.

2.3. Photometric Catalog

2.3.1. Matching Procedure

We used a near-final pre-release version of the SAGE catalog to obtain near- to mid-infrared photometry for our catalog of 1750 massive stars. The SAGE catalog includes the IRAC mosaic photometry source list, extracted from the combined epoch 1 and epoch 2 IRAC images and merged together with 2MASS and the 2MASS 6X Deep Point Source catalog (6X2MASS; Cutri et al. 2004), and the MIPS 24 μm epoch 1 catalog. The IRAC and MIPS 24 μm catalogs were constructed from the IRAC and MIPS 24 μm source lists after applying stringent selection criteria and are highly reliable. These catalogs are subsets of more complete, but less reliable archives. More details on the data processing and data products can be found in Meixner et al. (2006) and the SAGE Data Description Document⁴.

We extracted infrared counterparts to the massive stars in our list from the SAGE IRAC mosaic photometry catalog by performing a conservative neighbor search with a 1'' search radius and selecting the closest match for each source. This procedure yielded mid-infrared counterparts for 1316 of the 1750 sources. The IRAC mosaic photometry catalog, MIPS 24 μm catalog, IRSF, MCPS, and OGLE III catalogs were cross-matched in the SAGE database to provide photometry for sources over a wavelength range from 0.3 – 24 μm . We used this “universal catalog” to extract multi-wavelength photometry for IRAC sources matched to the massive stars. Specifically, for IRAC sources with one or more matches in other catalogs (all but 5), we only considered the closest matches between sources from any two available catalogs (IRAC–MIPS24, IRAC–MCPS, MIPS24–MCPS, IRAC–IRSF, MIPS24–IRSF, IRAC–OGLE III, MIPS24–OGLE III), with distances between the matched sources of $\leq 1''$. For example, for a match between the IRAC, MIPS 24 μm and MCPS catalogs (IRAC–MIPS24–MCPS), we applied these constraints on the IRAC–MIPS24, MIPS24–MCPS, and IRAC–MCPS matches. These stringent criteria were used to ensure that sources from individual catalogs for each multi-catalog match refer to the same star; they reduced the source list to 1262 sources. Six additional massive stars had matches within 1'' in the MIPS 24 μm Epoch 1 Catalog, but not in the IRAC Mosaic Photometry Catalog (IRACC). We supplemented the missing IRAC data: two sources had counterparts in the IRAC Mosaic Photometry Archive (IRACA) and 4 MIPS 24 μm sources had counterparts in the IRAC Epoch 1 Catalog (IRACCEP1). These IRAC sources were the closest matches to the MIPS 24 μm sources within 1''. Five out of 6 sources also have matches within 1'' in the MCPS catalog. Table 2 shows the breakdown of the matched stars to the catalogs, such that

⁴<http://irsa.ipac.caltech.edu/data/SPITZER/SAGE/doc/>

5 stars were only matched to the IRACC, 88 only to the IRACC+IRSF catalogs etc. The above requirements reduced the source list to 1268 sources⁵. We supplemented the missing IRAC data for 6 sources: two sources had counterparts in the IRAC mosaic photometry archive and 4 MIPS 24 μm sources had counterparts in the IRAC epoch 1 catalog. We defer the discussion of misidentifications and blending to §9.

2.3.2. Catalog Description

Table 3 presents our final matched catalog of 1268 stars, with the star name, IRAC designation, $UBVIJHK_s$ +IRAC+MIPS24 photometry and errors, reference paper, corresponding spectral classification and comments, sorted by increasing right ascension. Overall, the photometry is presented in order of shortest to longest wavelength. The 17 columns of photometry are presented in the following order: $UBVI$ from MCPS, VI from OGLE III, JHK_s from 2MASS, JHK_s from IRSF, IRAC 3.6, 4.5, 5.8, 8.0 μm and MIPS 24 μm . A column with the associated error follows each measurement, except for the OGLE III VI photometry. Henceforth, JHK_s magnitudes refer to 2MASS photometry, whereas IRSF photometry is denoted by a subscript, e.g. J_{IRSF} . All magnitudes are calibrated relative to Vega (e.g. see Reach et al. 2005, for IRAC). In Table 4, we summarize the characteristics of each filter: effective wavelength λ_{eff} , zero magnitude flux (in Jy), angular resolution, and the number of detected stars in each filter.

The spatial distribution of our 1268 matched sources is shown in Figure 1, overlaid onto the 8 μm image of the LMC. We find that the massive star population traces the spiral features of the 8 μm emission, which maps the surface density of the interstellar medium. Despite the fact that most studies we included from the literature targeted individual clusters, the spatial distribution of OB stars in our catalog is fairly uniform, with the exception of the N11, NGC 2004 and 30 Doradus regions, which have been subjects of several spectroscopic studies.

3. Color–Magnitude Diagrams

We divide the matched stars into 9 categories according to their spectral types: O stars, early (B0-B2.5) and late (B3-B9) B stars (the latter have supergiant or giant luminosity

⁵Preliminary estimates indicate that matches against the final catalog will not increase the number of matched stars by more than 1%.

classifications, except for 2 B3V stars), spectral type A, F and G (AFG) supergiants, K and M red supergiants (RSG), Wolf-Rayet stars (WR), supergiant B[e] stars (sgB[e]), confirmed luminous blue variables (LBV) and Be/X-ray binaries. In Figures 2 and 3, we present infrared $[3.6]$ vs. $[3.6] - [4.5]$ and $J - [3.6]$ color–magnitude diagrams (CMDs) for all the stars in the catalog, identifying stars in these 9 categories. The conversion to absolute magnitudes in all CMDs is based on a true LMC distance modulus of 18.41 mag (Macri et al. 2006). The locations of all the SAGE catalog detections are represented by the grey two dimensional histogram (Hess diagram). The red giants form the clump at $[3.6] > 15$ mag, while the vertical blue extension contains late-type LMC and foreground stars (free–free emission causes the OB stars to have redder colors). The asymptotic giant branch (AGB) stars are located at $[3.6] \sim 10$ mag, $J - [3.6] \sim 2.5$ mag. Immediately, one notices that the sgB[e], RSG, and LBVs stars are among the brightest stars at $3.6 \mu\text{m}$ and occupy distinct regions in the diagrams. Most of the O and B stars are located along a vertical line at $[3.6] - [4.5] \sim 0$, as expected. The RSG have “blue” colors because of the depression at $[4.5]$ due to the CO band (see e.g. Verhoelst et al. 2009). The WR stars are on average 0.3 mag redder than the OB stars because of their higher wind densities and, therefore, stronger free–free emission, while the sgB[e] stars are 0.6–0.7 mag redder and have similar brightnesses to the RSG. The Be/X-ray binaries are located among the “red” early-B stars. The LBVs have similar colors to the WRs, but are brighter. The late-B stars are brighter than the early-B stars because most of the former are luminous supergiants. The brightest of the AFG supergiants is the (only) G-type supergiant Sk $-69^{\circ}30$. A reddening vector for $E(B - V) = 0.2$ mag is shown in Figure 3 to illustrate the small effect of reddening, which decreases at longer wavelengths.

In Figures 4 and 5, we present $[8.0]$ and $[24]$ vs. $[8.0] - [24]$ CMDs, respectively. At these wavelengths, only stars with dust are detected, as the sensitivity of *Spitzer* drops sharply, while the flux from hot stellar photospheres also decreases. Therefore only the dusty WR, LBVs, sgB[e], and RSG are detected, as well as certain OB stars and late B and AFG supergiants, which are likely associated with hot spots in the interstellar medium, and may well be interacting with it. See §6, 7, 8, and 9 for a more detailed description of their colors. Stars with cool dust are brightest at $24 \mu\text{m}$, while emission from warmer dust peaks at $8 \mu\text{m}$. In these CMDs, the locations of the massive stars overlap with those of AGB stars, young stellar objects and planetary nebulae. Infrared colors alone are not sufficient to distinguish among these very different types of stars, illustrating the important diagnostic value of wide-baseline photometry.

4. Two-Color Diagrams

In Figures 6, 7 and 8 we present two-color diagrams (TCDs) using the near and mid-infrared photometry from our matched catalog. We label stars according to their spectral types and overplot all the SAGE detections in grey as Hess diagrams. We find that the majority of the OB stars have colors near zero in all bands, as expected, while there is an almost continuous extension of OB star “outliers” toward the WR stars, due to thick winds or the presence of disks. Among these outliers are the Be/X-ray binaries and other emission line stars. The most conspicuous group of stars in all TCDs are the B[e] supergiants, which have large excesses, of ~ 4 mag in the $K - [8.0]$ color. The RSG occupy a distinct position in the CMDs, because of their cooler temperatures, but are found to have a range of mid-infrared colors due to the amount of dust they contain (see §9). We have overplotted 6 simple theoretical models to guide the interpretation of the stars in these diagrams. These models are:

(i) Blackbodies (BBs) at 30,000, 10,000, 5,000, 3,000, 1,700, 1,100, 800 and 500 K. BBs are a good approximation of stellar emission in the infrared for most stellar atmosphere spectral energy distributions (SEDs), with the possible exception of red supergiants, which have spectra dominated by emission lines.

(ii) A power law model $F_\nu \propto \nu^\alpha$, for α ranging from -1.5 to 2 in steps of 0.5 . In the infrared, most stellar SEDs are close to the Rayleigh-Jeans tail of a BB and correspond to $\alpha \simeq 2$. As clearly illustrated by Panagia & Felli (1975) and Wright & Barlow (1975) (see also Panagia 1991), ionized stellar winds display flatter SEDs than BBs. This is because at low optical depths the gas emission in the wind (mostly free-free emission) is rather flat, and in the optically thick regime the increase of the size of the emitting region as a function of wavelength (e.g. $R \propto \lambda^{0.7}$ for a constant velocity wind) partially compensates for the intrinsic thermal λ^{-2} behaviour. Wind SED indexes asymptotically reach $\alpha = 0.6$ in the case in which *both* the expansion velocity is constant (e.g. at suitably large radii where the terminal velocity has been attained) *and* the optical depth is high (e.g. long wavelengths).

(iii) A model comprising a 30,000 K blackbody and an ionized wind. This approximates the case of all early-type stars (essentially OB and WR types) whose winds add a flatter spectral component that is noticed as an excess which becomes more conspicuous at longer wavelengths. Calculations were made following Panagia (1991) prescriptions for a spherically symmetric wind whose expansion velocity increases with radius like a power law, $v = v_o(r/r_o)^\gamma$, and for a wide range of mass-loss rates. Although these power laws represent just a zero-order approximation to the actual velocity structure of the wind (most noticeably, lacking a limiting/terminal velocity behaviour as suggested by ultraviolet line studies), they are able to reproduce the power-law behaviour of the wind SEDs in the regime of high optical

depths, i.e. where the wind contribution becomes dominant. For the sake of simplicity, we show here only the curves corresponding to $\gamma = 0.5$ and $\gamma = 0$. Since the gas opacity is an increasing function of the wavelength, for each given mass-loss rate, the wind emission is higher at long wavelengths. As a result the corresponding trajectories on the various TCDs are curves that start at the colors appropriate for a pure stellar SED (a power law $\alpha \simeq 2$), end at the asymptotic slope for very optically thick winds (e.g., 0.95 for $\gamma = 0.5$ and 0.6 for $\gamma = 0$), and display a characteristic upward concave curvature because of a more prompt increase in the redder colors (i.e. a positive second derivative). This is the only model not labeled in Figures 7 and 8, due to space constraints.

(iv) A model comprising a 30,000 K blackbody plus emission from an optically thin ionized nebula. Since the angular resolution of *Spitzer* is never better than $1.''7$, which at the LMC distance corresponds to more than 0.4 pc, we have to consider the case of an unresolved HII region surrounding an early-type star. For these models we adopted the gas emissivity as computed by Natta & Panagia (1976), which includes emission lines, bound-free and free-free continuum for both H and He, and is almost constant over the entire wavelength range $1 - 20 \mu\text{m}$. As expected, the curves start from the bare atmosphere point and asymptotically tend to a point corresponding to a spectral slope of $\alpha \sim 0$, displaying an upward concave curvature.

(v) A model with a 30,000 K blackbody plus cool dust emission (140 K and 200 K BB) with the amount of dust increasing in logarithmic steps of 0.5. This model may illustrate the case of an early-type star surrounded by a cool dusty envelope, perhaps similar to a sgB[e] star (Kastner et al. 2006), or stars with cold dust in their vicinity. In these calculations the dust opacity is assumed to be inversely proportional to the wavelength ($\kappa_{dust} \propto \lambda^{-1}$). At these dust temperatures the peak of the dust emission occurs at about 18 and 26 μm , and, therefore, the corresponding dust SED is rapidly (almost exponentially) increasing toward longer wavelengths, thus displaying a very negative slope ($\alpha \ll 0$).

(vi) A model with a 3,500 K blackbody plus 250 K dust, which was selected to represent the case of red supergiants (according to the new RSG effective temperature scale for a M3 I in the LMC, see Levesque et al. 2007). Also in these calculations the dust opacity is assumed to be inversely proportional to the wavelength ($\kappa_{dust} \propto \lambda^{-1}$), and the amount of dust is increased in logarithmic steps of 0.5. As expected, the starting point corresponds to the bare stellar atmosphere and the ending point is where the dust emission dominates (the peak of the dust emission SED occurs at about 15 μm), and the tracks display a typical upward concave curvature.

From these simple models and considerations, it appears that ionized gas emission produces a SED that declines with wavelength less steeply than a blackbody, thus possibly

causing an excess both in the infrared and in the radio domains but without reversing the overall declining trend of the SED. It follows that an observed flux increase toward longer wavelengths *necessarily* requires the presence of an additional component that has a suitably low temperature (e.g. less than 500 K for an upturn around $5 \mu m$) and has a suitably high emission to affect, and eventually dominate the observed SED. These properties correspond to the characteristics of a dusty layer, that is able to absorb mostly optical and ultraviolet photons and reradiate that energy in the infrared.

The locations of WR, LBV, sgB[e] and RSG are discussed in §6, 7, 8 and 9, respectively.

5. Infrared Excesses in OB stars

The primary cause of mid-infrared excess in OB stars is free–free emission from winds or disks. Since this emission is a monotonically increasing function of the optical depth that depends on the square of the electron density, one may find a different mid-infrared emission from stars with identical mass-loss rates but different wind velocity fields. Therefore, winds that are slow, clumped (e.g., Blomme et al. 2003) or compressed toward the equatorial plane to form a disk (Owocki et al. 1994) will have stronger mid-infrared emission. Given the sensitivity to these parameters, Castor & Simon (1983) and Abbott et al. (1984) concluded that mid-infrared emission alone cannot be used to determine the mass-loss rates of OB stars. More recently, Puls et al. (2006) argued that this very sensitivity makes mid-infrared emission extremely important in disentangling the nature of clumped winds. We therefore proceed to examine the mid-infrared excesses of the 354 O and 586 early-B stars in our photometric catalog.

In Figures 9 and 10, we plot J_{IRSF} vs. $J_{IRSF} - [3.6]$, $J_{IRSF} - [5.8]$ and $J_{IRSF} - [8.0]$ colors for O and early-B stars, respectively, indicating their luminosity classes, binarity and emission line classification properties by different symbols. We compare the observed colors with colors of plane-parallel non-LTE TLUSTY stellar atmosphere models (Lanz & Hubeny 2003, 2007) of appropriate metallicity and effective temperatures. We have not dereddened the stars, because this requires BV photometry of higher accuracy than that provided by the MCPS catalog; however, the low extinction toward the LMC ($\overline{E(B - V)} = 0.14$ mag; Nikolaev et al. 2004) makes such corrections small, as illustrated by the reddening vectors. For reference, TLUSTY models reddened by $E(B - V) = 0.2$ mag are also shown. We clearly detect infrared excesses despite not having dereddened the stars. At longer wavelengths, the excess is larger because the flux due to free–free emission for optically thin winds remains essentially constant with wavelength. Fewer stars are detected at longer wavelengths primarily because of the decreasing sensitivity of *Spitzer* and the overall decline of the SED.

We find that for $J < 13$ mag, more luminous OB stars exhibit larger infrared excesses in all colors due to winds. This can easily be understood considering that the infrared excess is an increasing function of the infrared optical depth, which in turn is proportional to the ratio $\dot{M}^2/(v_{exp}^2 R_*^3)$ (e.g. Panagia 1991). In early-type stars the mass-loss rate is found to be proportional to a power k (higher than unity) of the stellar luminosity, i.e. $\dot{M} \propto L^k$ with $k \simeq 1.2 - 1.6$ (Lamers & Leitherer 1993; Scuderi et al. 1998). The average expansion velocity is a function of the effective temperature, ranging from an initial value at the photosphere $v_0 \simeq v_{sound} \propto T_{eff}^{1/2}$ to a terminal value $v_\infty \propto T_{eff}^2$ (Panagia & Macchetto 1982), so that approximately $v_{exp} \simeq (v_0 v_\infty)^{0.5} \propto T_{eff}^{1.25}$. Since the stellar radius can be expressed as $R \propto L^{1/2}/T_{eff}^2$, it follows that the infrared optical depth in early-type star winds is proportional to $L^{(2k-1.5)} \times T_{eff}^{3.5}$, i.e. a $\sim 0.9 - 1.7$ power of the luminosity. This result can straightforwardly account for the observed increase of the infrared excess as a function of luminosity for O and B type stars in the LMC. We would like to mention that our findings confirm and provide a simple explanation for the luminosity effect between hypergiants and dwarfs noted by Leitherer & Wolf (1984) in their sample of 82 Galactic OB(A) stars. The brightest stars with the largest excesses shown in Figure 9 are late O supergiants, with large \dot{M} and low v_∞ . The spread in excesses at any given J -band magnitude (~ 0.2 mag at $J - [3.6]$, ~ 0.4 mag at $J - [8.0]$) cannot be due to reddening, which would displace all OB stars in a similar fashion. It is most likely related to the range of mechanisms that produce free-free emission, the properties of the winds (\dot{M} , v_∞ , clumping factors) and stellar rotation rates.

Stars with $J > 13$ mag that exhibit large excesses in Figure 9 are classified as emission line Oe/On/One, i.e. with evidence of fast rotation or circumstellar disks. In Figure 10, a larger fraction of stars with $J > 13$ mag are found to have large excesses, reflecting the higher fraction of emission line stars among B-stars compared to O-stars (Negueruela et al. 2004). The “B extr” stars (Schild 1966; Garmany & Humphreys 1985; Conti et al. 1986) are found to occupy similar parts of the CMD as the Be(Fe II) stars (notation by Massey et al. 1995) and Be-Fe stars (notation by Evans et al. 2006) (and also Be/X-ray binaries), suggesting these are objects of one and the same nature, with the presence of Fe II lines perhaps due to higher densities in the circumstellar disks. We note that some Be stars do not exhibit excesses, while several stars not classified as Be stars have excesses. Variability (disk dissipation), disk orientation, or insufficient spectral coverage leading to inaccurate classifications can explain these outliers. Therefore, infrared CMDs of optically blue selected stars can be used to identify new Be stars. An alternate explanation for some of the outliers is the new class of double periodic variables (or DPVs; Mennickent et al. 2003, 2005, 2008). DPVs are evolved B and A-type giants in an Algol mass-transfer configuration with circumprimary and circumbinary disks. These disks are thought to be responsible for the observed long period variability and infrared excess detected in the near-infrared.

5.1. OB star SEDs

Ultimately, the position of a star in a two-color or color-magnitude diagram is the result of its SED and luminosity, and it is the SED that can help us interpret its position in terms of its physical properties. Using the $0.3 - 24 \mu\text{m}$ photometry from Table 3, we created SEDs for the stars by converting their magnitudes to fluxes⁶. We used effective wavelengths and calibrations from Bessell et al. (1998) for *UBVI*, Rieke et al. (2008) for the 2MASS *JHK_s* and IRSF, Reach et al. (2005) for the *Spitzer* IRAC bands, and the *MIPS Data Handbook*⁷ for the MIPS $24 \mu\text{m}$ band. We compared the observed SEDs with models to assess the infrared excesses in the OB stars. TLUSTY models for LMC metallicity, a micro-turbulent velocity of 10 km s^{-1} , and the lowest available surface gravity for each effective temperature T_{eff} were selected to correspond to supergiant stars. The exact value of $\log g$ has little effect on mid-infrared fluxes for models with $T_{\text{eff}} \geq 25\text{kK}$ and, while larger, the effect remains $\lesssim 0.1 \text{ mag}$ in $(J - \lambda)$ (for $\lambda \geq 2.2 \mu\text{m}$) for the cooler models. We did not attempt to fit the SEDs, but simply overplotted models to provide a benchmark for determining the deviation of the observed SEDs from a “bare” photosphere. Deviations of OB stars from a TLUSTY model are due to reddening and free-free emission from their stellar winds.

Figure 11 shows representative SEDs for 10 OB stars, normalized by the flux at the *J*-band. The MCPS, IRSF and SAGE measurements (filled circles), and the 2MASS and OGLE photometry (open circles) are connected by a solid line. TLUSTY models, similarly normalized, are overplotted as solid lines, while the dotted lines correspond to the models reddened by $E(B - V) = 0.25$ and 0.50 mag (see the Appendix for details on the treatment of interstellar extinction). In Figure 12, we plot the same SEDs, divided by the unreddened TLUSTY models. These unitless plots make deviations from models obvious by avoiding the enormous flux ranges encountered when plotting the SEDs of hot stars in the mid-infrared. This ease of inspection comes with a price: when plotted against logarithmic wavelength, equal bins on the abscissa do not correspond to equal energy intervals. However, in these plots, the effects of reddening (clearly seen in the optical), infrared excess (detected in most cases) and even variability between the 2MASS-IRSF and OGLE III-MCPS photometry are clearly seen.

The O stars shown in the left panels of Figures 11 and 12 include the lightly reddened, luminous and hot star Sk $-70^\circ 91$, (O2 III(f*)+OB), which only has a weak infrared excess, in spite of having very strong ultraviolet P-Cygni wind lines ($v_\infty = 3150 \text{ km s}^{-1}$; e.g.

⁶Note, both magnitudes and fluxes exist in the SAGE database, but only magnitudes are included in our photometric catalog. Table 4 can be used to convert to fluxes.

⁷<http://ssc.spitzer.caltech.edu/mips/dh>

Massa et al. 2003). In such stars, the wind density remains low, creating only weak infrared emission. In contrast, the O4-5 V((f))pec star Sk $-70^\circ 60$ and the O6 Iaf+ star Sk $-65^\circ 22$ (with $v_\infty = 1350 \text{ km s}^{-1}$) have strong infrared excesses. The following two stars: Sk $-66^\circ 110$ and BI 192, are lightly reddened O9 I and O9 III stars, respectively, with distinctive evidence for infrared emission from their winds. These examples demonstrate that mass-loss rates cannot be derived solely from infrared excesses; an estimate of the spectral type and luminosity class is also required. We show examples of B giant and supergiant stars in the right panels of Figures 11 and 12. The B0 Ia star Sk $-68^\circ 52$ is not consistent with the SED of a reddened 30kK model, but shows evidence for infrared emission from a wind. Contrast the B0 III star Sk $-67^\circ 210$, which appears to be nearly unreddened, to the moderately reddened B0 III star ST2-46, exhibiting infrared excess. Sk $-68^\circ 8$ (B5 Ia+), compared to a 15kK model, similarly shows an infrared excess. The final SED is of Sk $-66^\circ 12$ (B8 Ia), also compared to a 15kK model (the coolest TLUSTY model available). While the star is probably cooler than 15kK, the reduction of the effective temperature by a few kK cannot account for the strong infrared excess, which is consistent with free-free emission from a wind. Careful modeling of each star will be necessary to accurately derive their wind properties.

6. Wolf-Rayet stars

Of the 125 WR stars in the catalog of Breysacher et al. (1999, not including BAT99-106 and BAT99-108 through BAT99-112 in the crowded R136 cluster), 99 yield matches in the SAGE database⁸. However, BAT99-45 and BAT99-83 are LBVs and BAT99-6 is an O star binary (given its O3f*+O spectral type; Niemela et al. 2001). Only 3 of the remaining 96 WR stars were detected at $24 \mu\text{m}$: BAT99-22 (WN9h), BAT99-55 (WN11h), BAT99-133 (WN11h, a spectroscopic twin to the LBV BAT99-83 in minimum). Our catalog includes various WR subtypes found in the LMC: early and late WN stars (some with hydrogen present); early WC stars of WC4 subtype; and one WO3 star. While most WR stars are thought to be post-main sequence stars with progenitor masses greater than $25 - 75 M_\odot$ (depending on the subtype; Crowther 2007), there is increasing evidence that the late-type WN stars with hydrogen in their spectra are hydrogen-burning stars with initial masses above $40 - 60 M_\odot$ (the lower initial mass being uncertain; Smith & Conti 2008). Studies by Bartzakos et al. (2001), Foellmi et al. (2003), and Schnurr et al. (2008) found the fraction of spectroscopic binaries among the WR stars in the LMC to be lower than expected. Given the diverse properties of objects encompassed under the “WR” classification, one might expect the position of WR stars on a CMD or TCD to depend on their spectral types and possibly be influenced by binarity.

⁸We label the B0 I + WN3 star Sk $-69^\circ 194$ (Massey et al. 2000) as an early-B star in our plots.

We examine the position of the WR stars on the J vs. $J - [3.6]$ CMD (Figure 13) as a function of their spectral type, subdividing them into: WN2-5, WN6-7, WN8, WN9-11, WC4 and WO3 and labeling the known binaries. On average, the WN6-7 and WN9-11 stars are more luminous and therefore brighter at J , when compared to their early WN2-5 counterparts. In particular, the late WN9-11 stars containing hydrogen are the brightest at J . These are the most luminous evolved WN stars, thought to be quiescent states of massive LBVs (Bohannon & Walborn 1989; Smith et al. 1994). Overall, the WR stars span 6 mag in J , and 2 mag in $J - [3.6]$ color, with the brighter stars being “bluer”, i.e. with steeper SEDs (see below). The brightest star is BAT99-22 (R84 or Sk $-69^\circ 79$) with a WN9h spectral type, which is known to be blended with a red supergiant (Heydari-Malayeri et al. 1997), while the reddest star is BAT99-38 (HD 34602 or Sk $-67^\circ 104$), a triple system (WC4(+O?)+O8I; Moffat et al. 1990) with an associated ring nebula (Dopita et al. 1994), which is probably responsible for the infrared excess. Dust is known to form around some colliding wind binary WC stars (see references in Crowther 2007), and was recently detected in the vicinity of WN stars (Barniske et al. 2008). The $24 \mu\text{m}$ detections around the WN11h stars BAT99-55 and BAT99-133, if confirmed, provide additional examples of WN stars with associated dust.

In Figure 14, we examine the colors of the WR stars in a $J - K_s$ vs. $K_s - [8.0]$ plot, following Hadfield et al. (2007). The location of LMC WR stars does not agree with the region Hadfield et al. (2007) defined by dashed lines to represent colors of Galactic WR stars. There are two reasons for this: 1) the Galactic sample includes many dusty WC9 stars that are intrinsically reddened (Gehrz & Hackwell 1974), and 2) line-of-sight reddening has scattered the Galactic sample into the region these authors have defined. Metallicity is not expected to affect the colors of WR stars, in particular WC stars, whose winds consist of processed and therefore enriched material. The WR stars define a rather narrow linear trend, independent of spectral type, defined by: $0 < J - K_s < 0.7$ mag and $0.4 < K_s - [8.0] < 2.0$ mag, corresponding to power law spectra with indexes $\alpha = 1.5$ to 0.5 , i.e. optically thick winds with modest velocity gradients (e.g. Panagia 1991). Single WR stars are expected to have flatter SEDs than binaries, which typically have main-sequence companions with steeper SEDs. The outliers in this plot are once again the heavily reddened WC4 triple system BAT99-38 and the blended star BAT99-22 (R84), whose infrared spectrum is dominated by the red supergiant. R84 is an outlier in all the CMDs, located among the RSG. On the $[3.6] - [4.5]$ vs. $[4.5] - [8.0]$ TCD (Figure 7) the WR stars follow a similar linear trend. We note that the brightest WR stars in J are the bluest in the TCDs.

In Figure 15, we show SEDs for 7 WR stars with representative subtypes. The strong C IV and He II emission lines present in the WO3 and WC4 stars (see Breysacher et al. 1999) are responsible for the “kinks” in the SEDs of these stars. For 3 of these stars (BAT99-123, BAT99-61, BAT99-17) we show model fits derived from mainly optical and near-infrared

spectroscopy using the spherical, non-LTE, line-blanketed CMFGEN code of Hillier & Miller (1998). For BAT99-123 (WO3), we use the model presented in Crowther et al. (2000) which is derived from line profile fits to ultraviolet and optical spectroscopy. This model has parameters of $T_{\text{eff}} = 150$ kK, $\log L/L_{\odot} = 5.3$, $v_{\infty} = 4,100$ km s $^{-1}$ and $\dot{M} = 1 \times 10^{-5} M_{\odot}$ yr $^{-1}$ for a volume filling factor of 0.1. For BAT99-61 (WC4), we use the model presented by Crowther et al. (2002) which has $T_{\text{eff}} = 52$ kK, $\log L/L_{\odot} = 5.68$, $v_{\infty} = 3,200$ km s $^{-1}$ and $\dot{M} = 4 \times 10^{-5} M_{\odot}$ yr $^{-1}$ for a volume filling factor of 0.1. For BAT99-17 (WN4o), we use the model summarized in Crowther (2006) which has $T_{\text{eff}} = 52$ kK, $\log L/L_{\odot} = 5.40$, $v_{\infty} = 1,750$ km s $^{-1}$ and $\dot{M} = 1.4 \times 10^{-5} M_{\odot}$ yr $^{-1}$ for a volume filling factor of 0.1. Overall, the model fits presented in Figure 15 show that the observed SEDs in the mid-infrared are flatter than the model continua, suggesting that either the model mass loss rates are too low or the winds are more highly clumped than the models predict. We caution, however, that this comparison is only for 3 stars. Generic CMFGEN models (Smith et al. 2002) are shown for the other 4 WR stars: a WN 85kK model for BAT99-1 (WN3b) and a WN 45kK model for the remaining WNL stars, all of which show excess above that predicted by the models. It is clearly desirable to investigate these apparent differences further by performing detailed line profile fits in the mid-infrared.

Finally, in Table 5 we present photometry for 10 WR stars with counterparts (within 20") at 70 μm and for 1 WR star with a counterpart at 160 μm . The star name, spectral type, magnitude and associated error at 70 μm and 160 μm , followed by the flux and associated error in these bands, are given. We caution that the angular resolution of MIPS is 18" and 40", respectively, at these bands. However, we note that the sgB[e] and LBVs detected also show evidence for dust at the IRAC+MIPS24 bands.

7. Luminous Blue Variables

There are 6 confirmed LBVs (see review by Humphreys & Davidson 1994) in the LMC: S Dor, BAT99-83 or R127, R 71, R 110, BAT99-45, and R 85, although another 5–6 have been suggested as candidates in the literature (see e.g., Weis 2003). The LBVs are not only among the most luminous sources at 3.6 μm (see Figure 2 and 3), with [3.6]–[4.5] colors similar to AGB stars and intermediate between RSG and sgB[e] stars, but also at 8.0 μm (Figure 4) and 24 μm (Figure 5). In the TCDs (Figures 6 and 7) the LBVs are located between the OB and WR stars, with the exception of R71 (Lennon et al. 1993), which is an extreme outlier, with $K_s - [8.0] = 3.4$ mag and $[4.5] - [8.0] = 2.5$ mag. Its recent brightening of 1.5 mag between 2006 and 2009 (see light curve from the *All Sky Automated*

*Survey*⁹; Pojmanski 2002) cannot account for its infrared colors. Instead, the emission from polycyclic aromatic hydrocarbons (PAHs) detected by Voors et al. (1999) in R71 can explain its “red” colors, since there are strong PAH lines in the [3.6] and [8.0] bands. All 6 confirmed LBVs were detected in the IRAC bands, 3 were detected in the MIPS 24 μm band and 2 at 70 μm : R71 (saturated at 24 μm) and BAT99-83 or R127 (see Table 5). The R71 detection is consistent with the 60 μm value in the IRAS Point Source Catalog and Voors et al. (1999) suggest that a combination of crystalline silicates and cool dust are responsible for it. The detection of R127 at 70 μm may imply that a similar dusty environment exists around this star. We note that BAT99-45 is distinctively “bluer” than the other two LBVs detected at 8.0 μm and 24 μm (see Figures 4, 5, 8).

The SEDs of all 6 confirmed LBVs are shown in Figure 15 and, unlike other classes of stars, are highly non-uniform. Since LBVs are by definition variable and the photometry in different bands was obtained at different epochs, the differences in the 2MASS and IRSF photometry are most likely due to variability. We only have MCPS photometry for two LBVs, which seems either variable or of suspect quality. S Dor, the prototype S Doradus variable, and R127 (in outburst during the SAGE observations; Walborn et al. 2008) are the brightest LBVs at 24 μm (Figure 5). Many LBVs are surrounded by small nebulae (0.2–2 pc) originating from past giant eruptions, which form cool dust. For example, R127 was found to have a bipolar nebula (Weis 2003). The dust associated with its nebula is likely responsible for the bright mid-infrared magnitudes of R127. R71 exhibits a strong excess in the IRAC bands, as expected from its position in the TCDs.

Do LBVs represent a homogeneous class of objects? Their infrared SEDs point to diverse properties, which is not surprising given their spectral variability during eruptions. On the one hand, the low luminosity LBV R71, with an estimated progenitor mass of around 40 M_{\odot} has one of the strongest infrared excesses of any massive star in the LMC and is well known as a source of dust emission. S Dor and R127 are more typical massive LBVs, both of which exhibit an infrared excess, possibly linked to circumstellar material formed during their recent outbursts. The other three LBVs in the sample: R110, BAT99-45 (also Sk -69° 142a, S83) and R85 all show different but coherent infrared behaviour more consistent with a stellar wind contribution only. It is possible that dust around these objects is cooler; however these stars were not detected at the longer MIPS bands. The different shapes of the LBV SEDs are likely related to the time since the last outburst event and the amount of dust formed.

⁹<http://www.astrouw.edu.pl/asas/>

8. B[e] supergiants and Classical Be stars

B[e] supergiants (sgB[e]) are a distinct class of B-type stars exhibiting forbidden emission lines, or the “B[e] phenomenon” (Lamers et al. 1998). They are characterized by strong Balmer emission lines, narrow permitted and forbidden low-excitation emission lines and a strong mid-infrared excess. A two-component wind model with a hot polar wind and a slow and cool equatorial disk wind has been proposed to explain them (Zickgraf et al. 1986); however models of the disk have so far achieved limited success (Porter 2003; Kraus et al. 2007; Zsargó et al. 2008). On the Hertzsprung-Russell (HR) diagram, sgB[e] stars are located below the Humphreys-Davidson limit (Humphreys & Davidson 1979), a few of them being coincident with the location of LBVs. However, the existence of an evolutionary connection of sgB[e] stars to LBV stars (transitional phase between Of and WR stars) is unclear. Langer & Heger (1998) outline three possible ways sgB[e] could form circumstellar disks: from single massive evolved stars close to critical rotation (Meynet & Maeder 2006), blue supergiants which have left the red supergiant branch, and from massive binary mergers (Podsiadlowski et al. 2006).

The sgB[e] stars are the most conspicuous group of stars in all infrared CMDs and TCDs: they are among the brightest and most reddened stars in the LMC (also noted by Buchanan et al. 2006). In the LMC, 12 stars have been classified as sgB[e] stars (including LH 85–10, although it is not among the 11 stars listed in Zickgraf 2006). The 11 that were included in our catalog (S 22, S 134, R 126, R 66, R 82, S 12, LH 85-10, S 35, S 59, S 137, S 93) were all matched in the SAGE database. Their SEDs are shown in Figure 16. The B0.5[e] stars are sorted by decreasing flux at [3.6], the later-type B[e] stars by decreasing effective temperature. A 25kK TLUSTY model representing the underlying photosphere is overplotted. We find that the SED of LH 85–10, a suspected LBV assigned a B[e] spectral type by Massey et al. (2000), resembles the SEDs of “classical Be” stars (Negueruela 2004). Figures 2, 3, 6, and 7 demonstrate that LH 85–10 is much fainter and less reddened than sgB[e] and LBV stars, and is located near Be stars, and therefore may have been misclassified as a B[e] star. The SEDs of the remaining 10 sgB[e] stars are all very similar, with slowly decreasing flux in the optical, an inflexion point in the near-infrared and a “bump” starting at $2 \mu\text{m}$ and peaking near $5 \mu\text{m}$. This peak corresponds to hot dust at $\sim 600 \text{ K}$. The slight change in the slopes of the SEDs between 8 and $24 \mu\text{m}$ from star to star suggests different contributions from cool dust (150 K). R66, S35 and R126 were also detected at $70 \mu\text{m}$ (Table 5). We find all 10 sgB[e] stars to be extinguished by $E(B - V) \gtrsim 0.5$.

Kastner et al. (2006) presented *Spitzer* IRS spectroscopy for 2 of these sgB[e] (R66,

R126¹⁰), finding evidence for massive circumstellar disks, which can simultaneously explain the (relatively) small amount of reddening in the optical and the observed infrared excess. However, the mass-loss rate required to sustain such a massive disk is very high and unlikely to persist during the He burning phase of the star. These authors argued against a model of episodic mass ejection based on the similarity of the SEDs of the two sgB[e] they studied. The similarity of all 10 sgB[e] SEDs makes the scenario of episodic mass ejection even less likely or, alternatively, suggests a shorter duration of the sgB[e] phase or even an origin in a binary companion. The small fraction of sgB[e] stars among B stars might present a clue to their origin. We note that the rare, dust obscured, luminous progenitors (Prieto et al. 2008; Prieto 2008) of the newly discovered class of transients, including SN2008S (Smith et al. 2009) and NGC 300 OT (Bond et al. 2009; Berger et al. 2009), could be related to the lower luminosity B[e] supergiants, given that both are likely post-main-sequence stars (possibly in a post-red supergiant phase) with dust and similar luminosities. Thompson et al. (2008) presented evidence for a short duration ($< 10^4$ yr) of the dust-enshrouded phase prior to eruption.

The infrared emission in the sgB[e] stars is much stronger than in classical Be stars (shown in Figure 17). It is typically several hundred times stronger than the photosphere at $8 \mu\text{m}$, and up to 1000 times stronger at $24 \mu\text{m}$, explaining the extreme positions of sgB[e] stars in the TCDs. In the classical Be stars, free-free emission from disks can cause the $8 \mu\text{m}$ flux to be 10 times that of the underlying photosphere, as is the case for all but one (Sk $-71^\circ 13$) of the Be stars shown. The emission in classical Be stars can be highly variable (see review by Porter & Rivinius 2003), which may account for the disagreement between the IRSF and 2MASS photometry for NGC 2004-033 (B1.5e), and in some cases, can even dissipate altogether, as for Sk $-71^\circ 13$ (Be (Fe-Be)). The SEDs of the remaining Be, “B extr”, Be (Fe-Be) stars are identical, thereby providing additional evidence (see §5) that these stars are the same objects: the most luminous of the Be stars. We also present the SED of 1 of the 4 Be/X-ray binaries in our matched catalog, finding it to have a peculiar shape, similar to the other Be stars, but with excess emission in the [3.6] and [4.5] bands, possibly due to variability.

¹⁰Note, the sgB[e] star R126 (Sk $-69^\circ 216$) is located in NGC 2050, close to the LBV R127 (Sk $-69^\circ 220$), which is in NGC 2055. These two clusters could be a “fossil” two-stage starburst.

9. Red Supergiants & Other Stars

The red K and M supergiants are among the brightest stars in the LMC at all infrared wavelengths. However at $24\ \mu\text{m}$ they span 5.5 magnitudes (see Figure 5). This is due to the different types and amounts of dust contributing to the SED at these wavelengths due to different mass-loss rates (see Verhoelst et al. 2009). Josselin et al. (2000) note that the $K - [12]$ color index is a mass-loss indicator; therefore, we similarly interpret the range in $[24]$ magnitudes and the 2 magnitude spread in $K_s - [8.0]$ color in Figure 6 as a reflection of the range of mass-loss rates. In Figure 8, we notice a temperature trend: red supergiants clustered at the bottom left (i.e. with “blue” colors) are predominantly K or early M supergiants, while the bulk of M0–M4 supergiants are found in a band, roughly following the RSG model described in §4. The temperature trend correlates with the optical depth of the dust emission and the amount of dust, which in turn is a function of the mass-loss. The offset from the blackbody model can be explained by dust; exceptions to this trend might be due to misclassifications, blends, or variability. The same temperature trend is seen in Figure 5, with the coolest RSG being the most luminous at $24\ \mu\text{m}$. Our catalog includes LMC 170452, which is a rare example of a RSG that has changed spectral types. Levesque et al. (2007) found it to vary from M4.5–M5 I in 2001 and 2004 to M1.5 I in 2005 December. The SAGE observations were also taken in 2005 (July & October), possibly during the transition. We suggest that supergiants not appearing to follow the temperature trend in Figure 8 could signify spectral variability (e.g. the “blue” M2 star [SP77]55-20 and the very red K0 star 165543). The extremely reddened (at long wavelengths) outlier in Figures 4, 5, and 8 is the M2-3 supergiant 175549 with $[8] - [24] = 4$ mag. The M0 I 138475 has $K_s - [8.0] = 3$ mag, making it an outlier in Figure 6. In Figure 3, it is located with the AGB stars, implying it is an M-type AGB star.

Figure 18 shows representative SEDs of yellow and red supergiants. The SED peak moves redward with decreasing temperature, as expected. Note that starting at Sk $-69^\circ 30$ (G5 I), a depression in the continuum due to the CO band appears at $4.5\ \mu\text{m}$, and persists to later types. This depression is extremely weak or absent in the M1 Ia, 138552. Some of the later supergiants have a distinct break in their slopes at roughly $4.5\ \mu\text{m}$, also coinciding with the CO band. The SED of LH 31-1002 (F2 I), suggests a hotter effective temperature, inconsistent with its spectral type. Massey et al. (2000) give $B - V = 0.4$ mag for this star, in disagreement with the value from MCPS ($B - V = -0.2$ mag), perhaps suggesting an error in its coordinates that lead to a match with a nearby hot star. The K7 I star 139027 also appears to have an excess at the shortest wavelengths; therefore it is a candidate ζ Aurigae binary (Wright 1970), with a hot companion. LMC 170452, has a peculiar SED (with $V - K = 7.2$ mag, instead of ~ 5), possibly reflecting its spectral type change.

Finally, in Figure 19 we present some peculiar SEDs, illustrating examples of nebular contamination (N11-081), variability (RXJ0544.1-7100), blending (BAT99-22) or misidentification (Sk -67° 29, Sk -70° 33) in our photometric catalog. Nebular contamination and misidentifications are responsible for the OB outliers in the CMDs and TCDs. Only 3 out of 354 O stars (N11-028, N11-046, lmc2-703– all main-sequence stars) and 15 out of 586 early-B stars have $24\ \mu\text{m}$ detections, illustrating that contamination is less than 3% at this wavelength.

10. Summary

This paper presents the first major catalogs of accurate spectral types and multi-wavelength photometry of massive stars in the LMC. The spectroscopic catalog contains 1750 massive stars, with accurate positions and spectral types compiled from the literature, and includes the largest modern spectroscopic surveys of hot massive stars in the LMC. The photometric catalog comprises uniform $0.3\text{--}24\ \mu\text{m}$ photometry in the $UBVIJHK_s$ +IRAC+MIPS24 bands for a subset of 1268 stars that were matched in the SAGE database. Our photometric catalog increases the infrared photometry for OB stars presented in a single study by an order of magnitude, allowing for a detailed study of their wind parameters. The low foreground reddening toward the LMC and the identical distance of the stars in the sample remove degeneracies inherent in Galactic studies and enable the investigation of infrared excesses, while minimizing systematic errors due to reddening.

We examine the infrared excesses of the half-solar metallicity OB stars in the LMC, finding a correlation of excess with wavelength, as expected, and luminosity. The dispersion in the relation reflects the range of mechanisms, and therefore stellar wind parameters, which produce free–free emission in OB stars. We discuss the positions of OB stars, WR, LBV, sgB[e], classical Be stars, RSG, AFG supergiants and Be/X-ray binaries on CMDs and TCDs, which serve as a roadmap for interpreting existing infrared photometry of massive stars in nearby galaxies. We conclude that sgB[e], RSG and LBVs are among the most luminous stars in the LMC at all infrared wavelengths. Representative SEDs are shown for all types of stars, and in certain cases are compared to model atmospheres to illustrate infrared excesses due to free–free emission from winds or disks. We confirm the presence of dust around 10 sgB[e] stars from the shape of their spectral energy distributions, which are presented for the first time at these mid-infrared wavelengths, and find the SED shapes to be very similar. The large luminosities and the presence of dust characterizing both B[e] supergiants ($\log L/L_\odot \geq 4$) and the rare, dusty progenitors of the new class of optical transients (e.g. SN 2008S and NGC 300 OT), suggest a common origin for these objects. The variety of

SED shapes observed among the LBVs is likely related to the time since the last outburst event and the amount of dust formed. Finally, we find the distribution of infrared colors for WR stars to differ from that of Galactic WR stars, due to the abundance of Galactic dusty WC9 types and the effects of foreground reddening in the Milky Way.

This work demonstrates the wealth of information contained in the SAGE survey and aims to motivate more detailed studies of the massive stars in the LMC. Examples of studies that can be conducted using our catalogs follow: (a) Candidate RSG, sgB[e], LBV in the LMC and other galaxies can be identified by selecting them from infrared CMDs, ruling out AGB stars from optical and near-infrared photometry (if it exists), and confirming these with spectroscopy. For example, in IC 1613, a comparison of the IRAC CMD in Figure 4 of Jackson et al. (2007b) to our Figure 2, suggests that the brightest “blue” stars are candidate RSG or LBV stars. With the optical catalog of Garcia et al. (2009), their visual colors can be determined and 0.3-8 μm SEDs can be constructed. (b) Specific stars or categories of stars can be selected from the catalog for further study. For example, mass-loss rates can be determined for OB stars that have spectra from the *Far Ultraviolet Spectroscopic Explorer* (e.g. Fullerton et al. 2000), since terminal velocities can be measured from the ultraviolet lines. (c) The OB stars can be used to determine the LMC reddening law, given the known spectral types and SED shapes of these stars. (d) Variability in 2MASS–IRSF photometry can be used to pick out new, variable, massive stars. The most luminous stars in our catalog ($V \sim 10$ mag) are saturated in the LMC microlensing surveys; however, the two epochs of near-infrared photometry can be used, for example, to find candidate eclipsing binaries not included in the OGLE (Wyrzykowski et al. 2003) or MACHO (Faccioli et al. 2007) lists. (e) Our catalog can be cross correlated with X-ray catalogs of the LMC to study non-thermal emission processes in massive stars.

A comparison of the infrared properties of massive stars in the Large vs. Small Magellanic Cloud (SMC) will be pursued next. Stellar winds scale with metallicity (Mokiem et al. 2007); therefore, a comparison of infrared excesses of OB stars in the LMC vs. the SMC will help quantify the effect of metallicity on OB star winds, Be star properties, sgB[e] stars etc. In the future, the *James Webb Space Telescope* will obtain infrared photometry of massive stars in galaxies out to 10 Mpc and measuring the colors of massive stars as a function of metallicity, will be useful for interpreting these data.

We acknowledge the input from members of the Massive Stars & Starbursts research group at STScI, in particular, Nolan Walborn. We thank Bernie Shao for incorporating the OGLE III photometry to the database and Paul Crowther for providing us with his CMFGEN models of WR stars. AZB acknowledges support from the Riccardo Giacconi Fellowship award of the Space Telescope Science Institute. The *Spitzer* SAGE project was

supported by NASA/*Spitzer* grant 1275598 and NASA NAG5-12595. This work is based [in part] on archival data obtained with the *Spitzer* Space Telescope, which is operated by the Jet Propulsion Laboratory, California Institute of Technology under a contract with NASA. Support for this work was provided by an award issued by JPL/Caltech. This publication makes use of data products from the Two Micron All Sky Survey, which is a joint project of the University of Massachusetts and the Infrared Processing and Analysis Center/California Institute of Technology, funded by the National Aeronautics and Space Administration and the National Science Foundation.

Facility: Spitzer (IRAC, MIPS)

Appendix

We adopted a reddening curve composed of a continuous contribution and a feature which represents silicate absorption at $9.7 \mu\text{m}$. The continuous portion is based on the formulation used by Fitzpatrick & Massa (2009) to fit near-infrared extinction curves (which include 2MASS JHK_s) and is a generalization of the analytic formula given by Pei (1992). For $\lambda \geq \lambda_0$, it has the form

$$k(\lambda - V)_c \equiv \frac{E(\lambda - V)}{E(B - V)} = \frac{0.349 + 2.087R(V)}{1 + (\lambda/\lambda_0)^\alpha} - R(V), \quad (1)$$

where $\lambda_0 = 0.507 \mu\text{m}$. The ratio of total to selective extinction, $R(V) \equiv A(V)/E(B - V)$, and α are free parameters. Near-infrared observations show that these parameters can vary from one sight line to the next. In this work, we use a curve defined by $\alpha = 2.05$ and $R(V) = 3.11$. These parameters provide a good representation of the mean curve determined by Fitzpatrick & Massa (2009) and also to extinction data taken from the literature for diffuse interstellar medium sight lines in the Milky Way. The latter data sets extend to $24 \mu\text{m}$ and include the following: Castor & Simon (1983), Koornneef (1983), Abbott et al. (1984), Leitherer & Wolf (1984), Rieke et al. (1989), Wegner (1994), and Nishiyama et al. (2009). Although we cannot be certain this same form applies to the LMC, it is consistent with the SEDs of lightly reddened, normal hot stars that are thought to have weak winds (see §5). In any case, the extinction for most of our objects is small enough that inaccuracies in the interpretation of reddening should be minimal. For completeness, we included a Drude profile (see, e.g., Fitzpatrick & Massa 2009) to describe the $9.7 \mu\text{m}$ silicate feature, even though it has little effect on the *Spitzer* bands. The adopted profile is given by

$$f(\lambda) = \frac{a_3 x^2}{(x^2 - x_0^2)^2 + (x\gamma)^2}, \quad (2)$$

where $x = 1/\lambda \mu\text{m}^{-1}$, and the parameters were assigned the values $x_0 = 1/9.7 \mu\text{m}^{-1}$, $\gamma = 0.03$ and $a_3 = 3 \times 10^{-4}$. Finally, the complete extinction curve is given by $k(\lambda - V) = k(\lambda - V)_c + f(\lambda)$. When we plot the SEDs, we actually use the form $k(\lambda - J) = k(\lambda - V) - k(J - V)$.

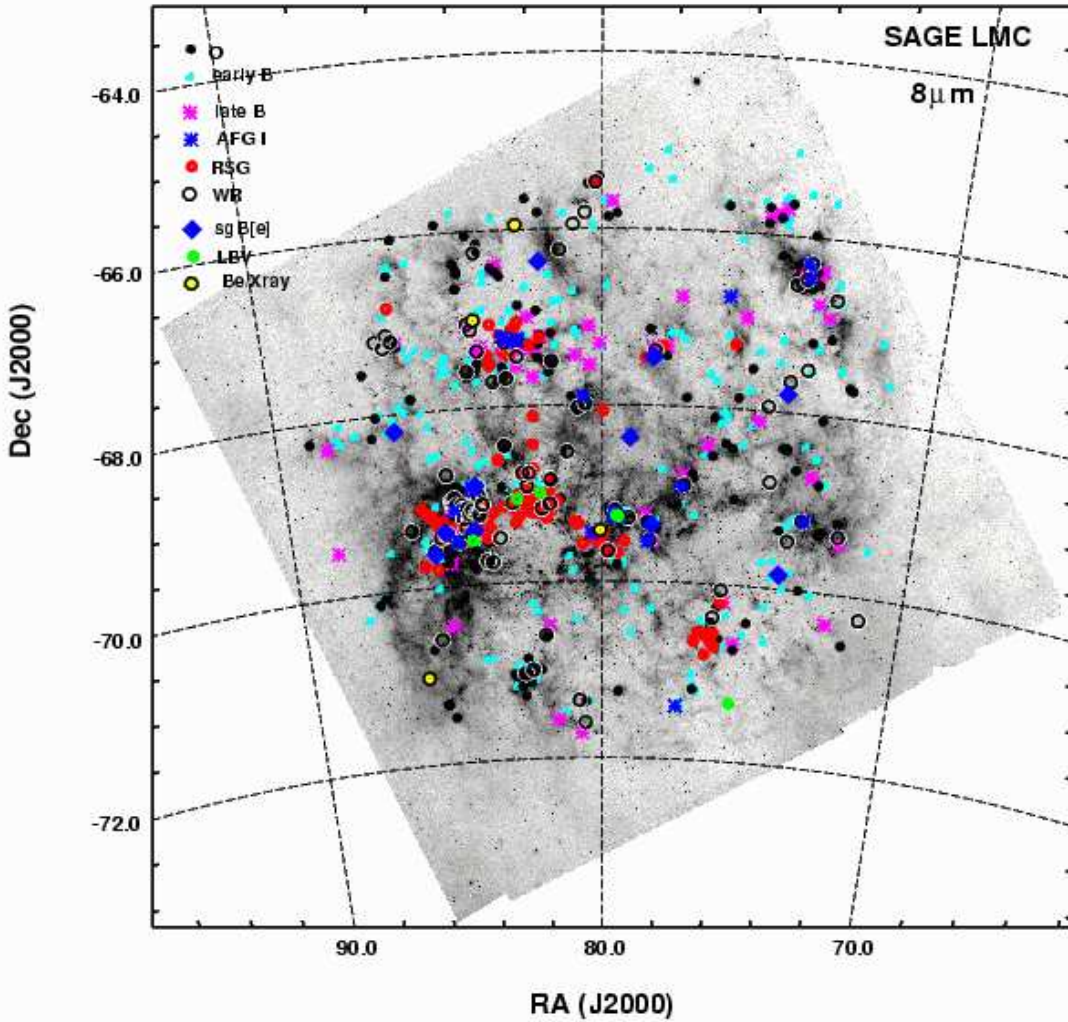


Fig. 1.— Spatial distribution of massive stars with IRAC counterparts, which are found to trace the spiral features in the $8\ \mu\text{m}$ SAGE mosaic image. Different symbols denote different spectral types. The spatial distribution of the OB stars is uniform, with the exception of the N11 (at $\sim 74^\circ$, -66.5°), NGC 2004 (at $\sim 82^\circ$, -67.3°) and 30 Doradus (at $\sim 85^\circ$, -69°) regions.

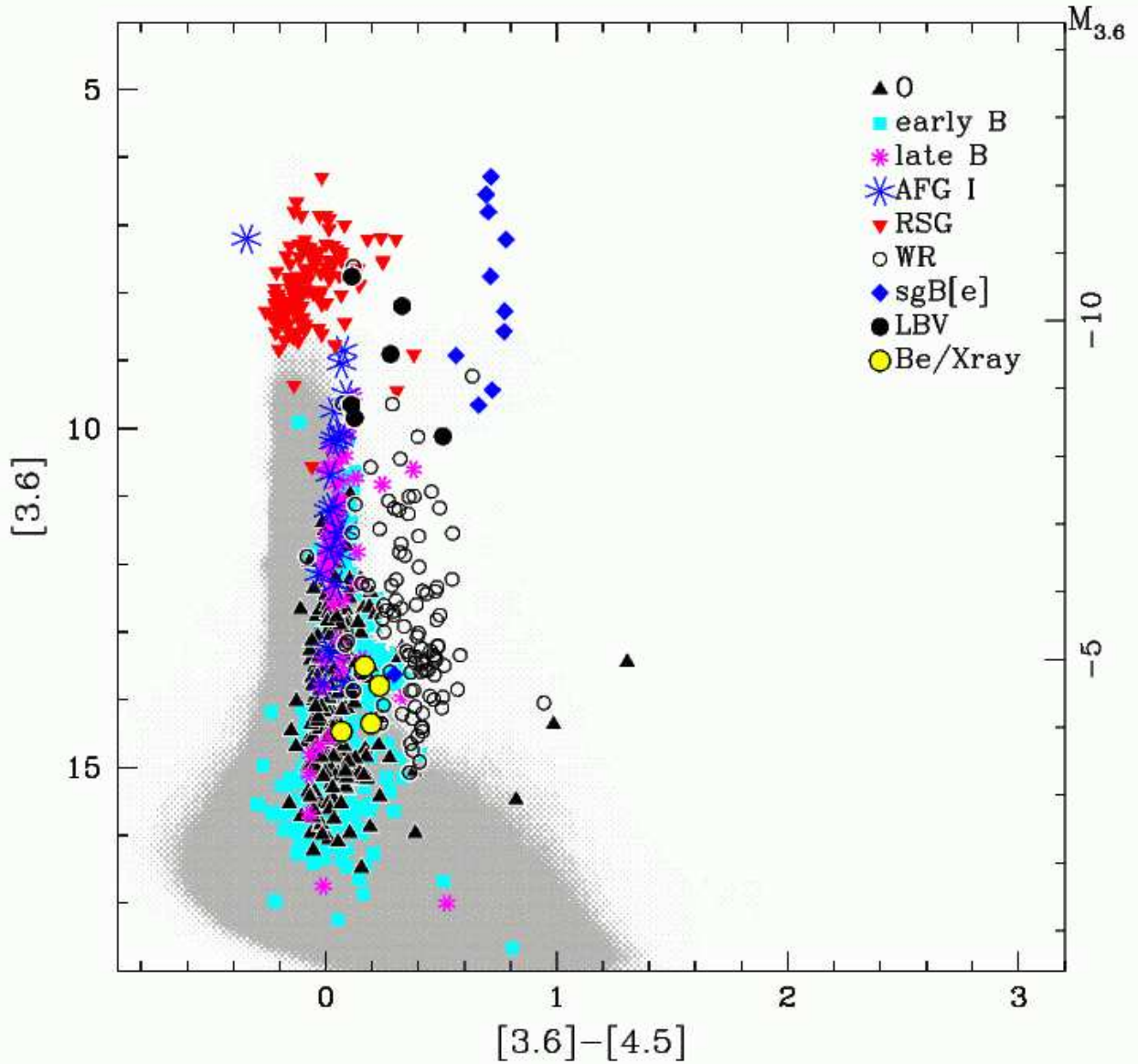


Fig. 2.— $[3.6]$ vs. $[3.6] - [4.5]$ color magnitude diagram for massive stars with IRAC counterparts in the SAGE database. The conversion to absolute magnitudes is based on a true LMC distance modulus of 18.41 mag (Macri et al. 2006). Different symbols denote different spectral types. The locations of all the SAGE detections are shown in grey as a Hess diagram. The sgB[e], RSG and LBVs are among the most luminous stars at $3.6 \mu\text{m}$.

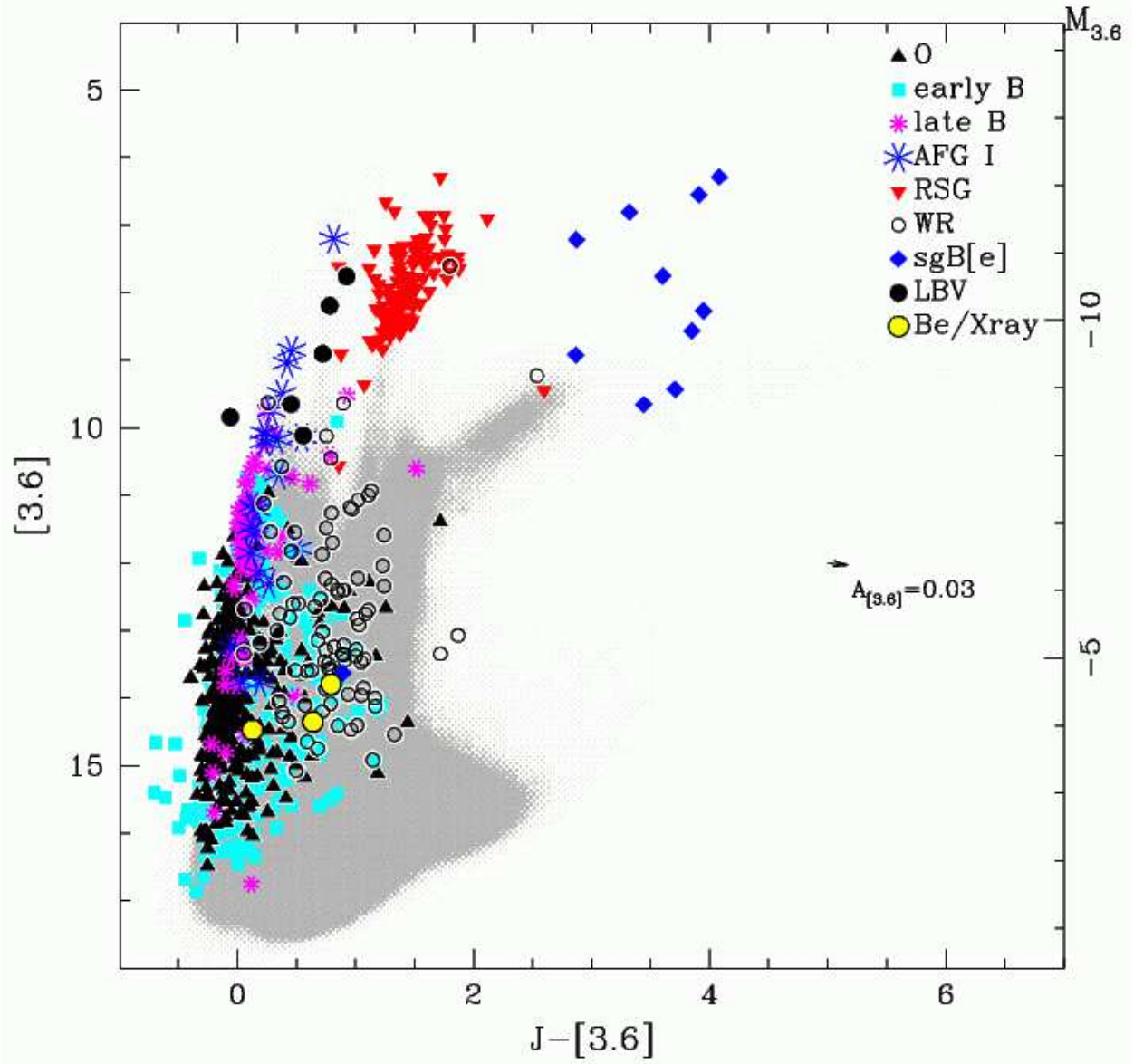


Fig. 3.— Same as Figure 2, but for the $[3.6]-J$ vs. $[3.6]$ color magnitude diagram. The longer baseline separates the populations more clearly. The reddening vector for $E(B - V) = 0.2$ mag is shown.

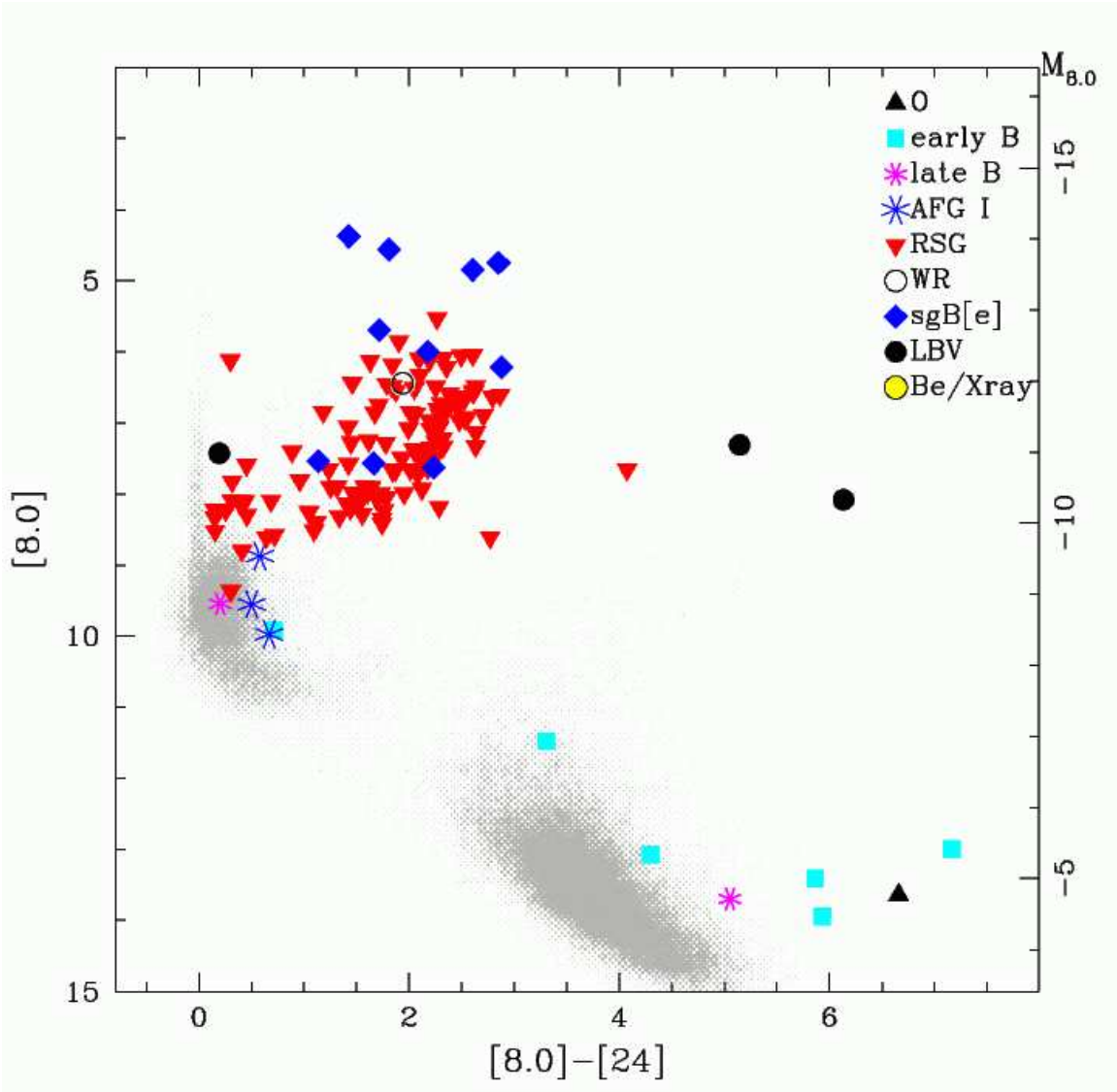


Fig. 4.— Same as Figure 2, but for the $[8.0]$ vs. $[8.0] - [24]$ color magnitude diagram. The sgB[e], RSG and LBVs are also among the most luminous stars at $8 \mu\text{m}$.

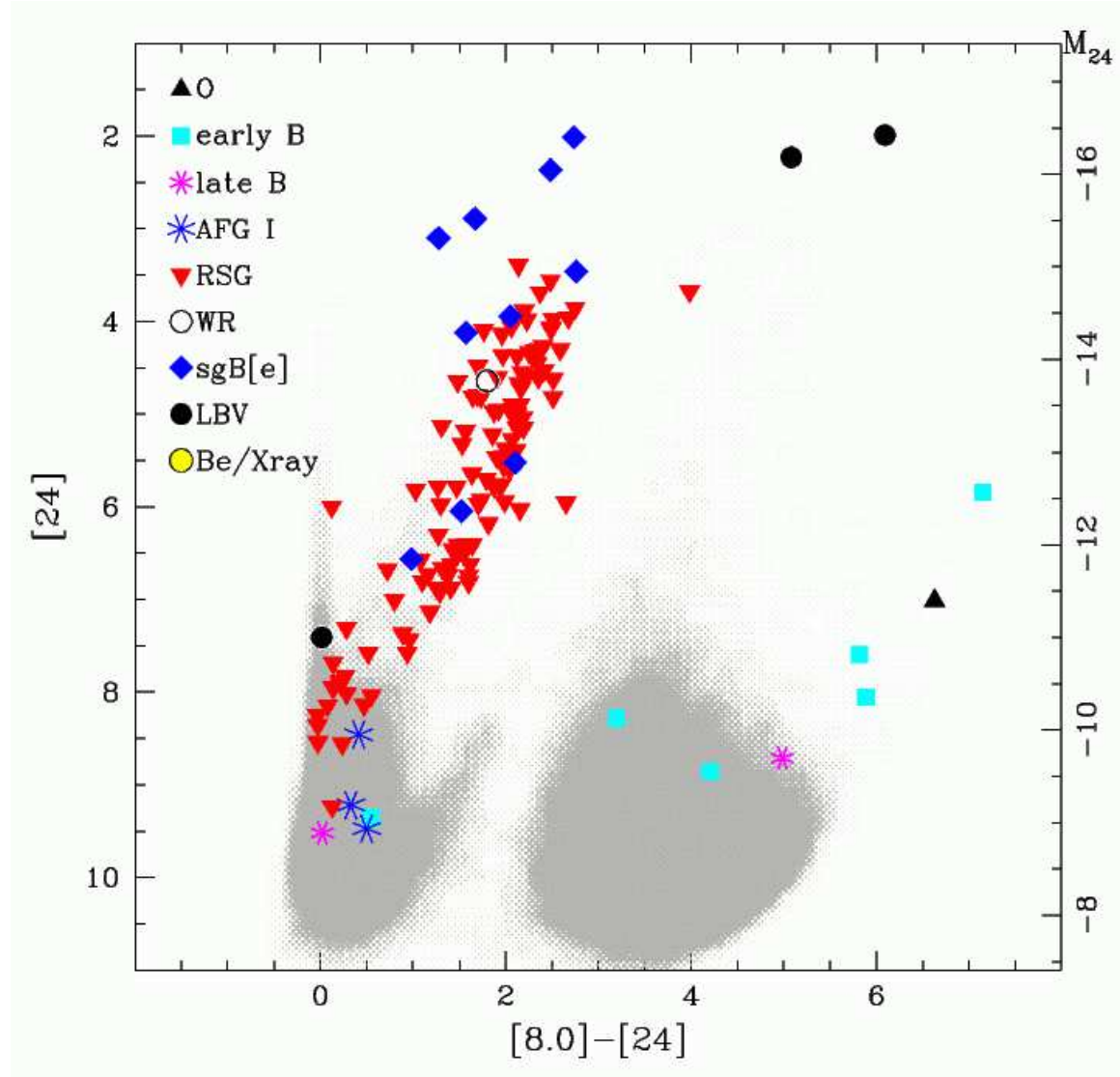


Fig. 5.— Same as Figure 2, but for the [24] vs. [8.0] - [24] color magnitude diagram. The brightest sgB[e], RSG and LBVs are among the most luminous stars at 24 μ m.

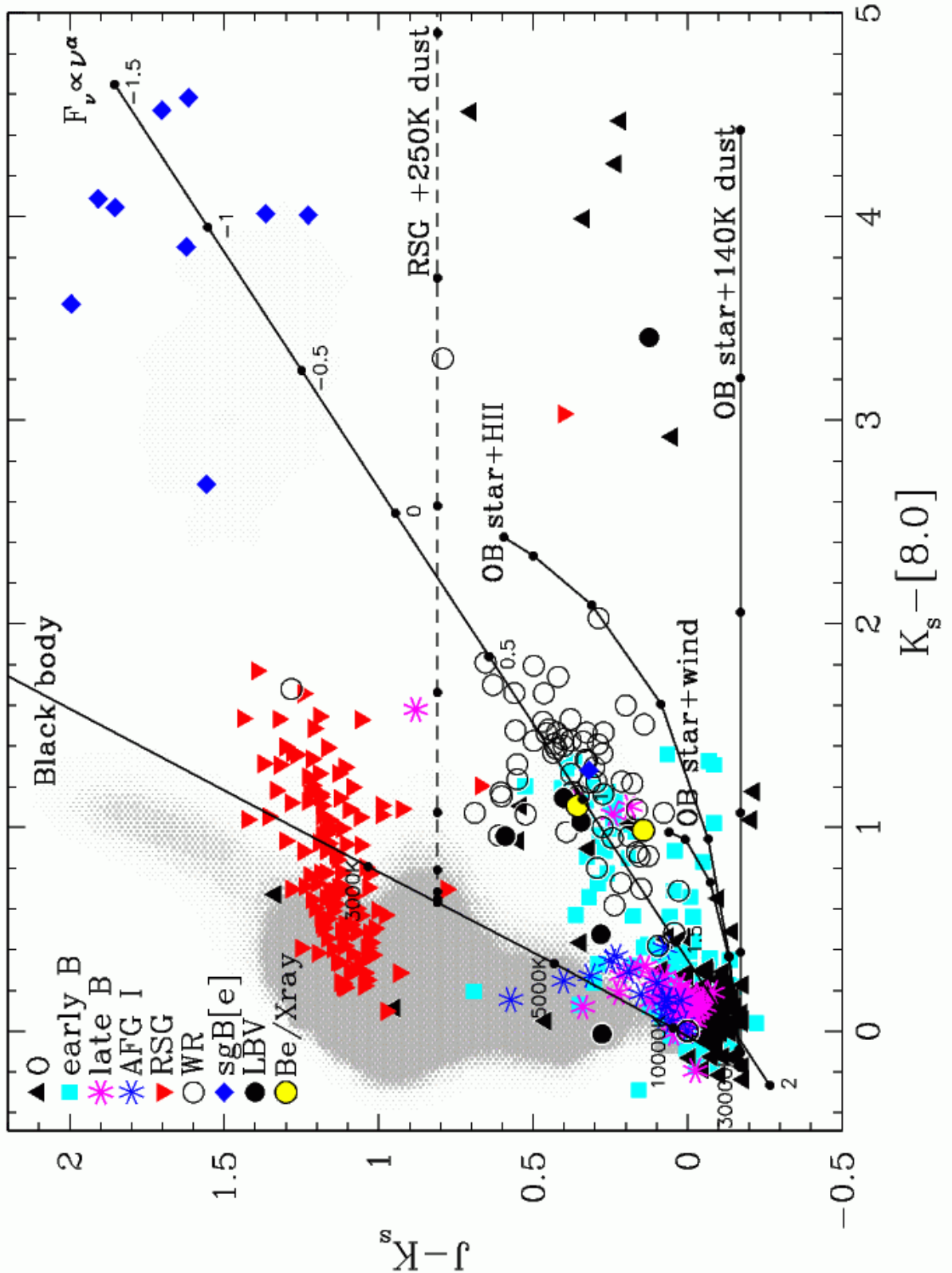


Fig. 6.— $J - K_s$ vs. $K_s - [8.0]$ diagram for massive stars in our catalog. The locations of all the SAGE detections are shown in grey as a Hess diagram. The solid lines represent models (described in §4): (i) a BB at various temperatures, as labelled, (ii) a power law model $F_\nu \propto \nu^\alpha$, for $-1.5 < \alpha < 2$, (iii) an OB star plus an ionized wind (not labelled),

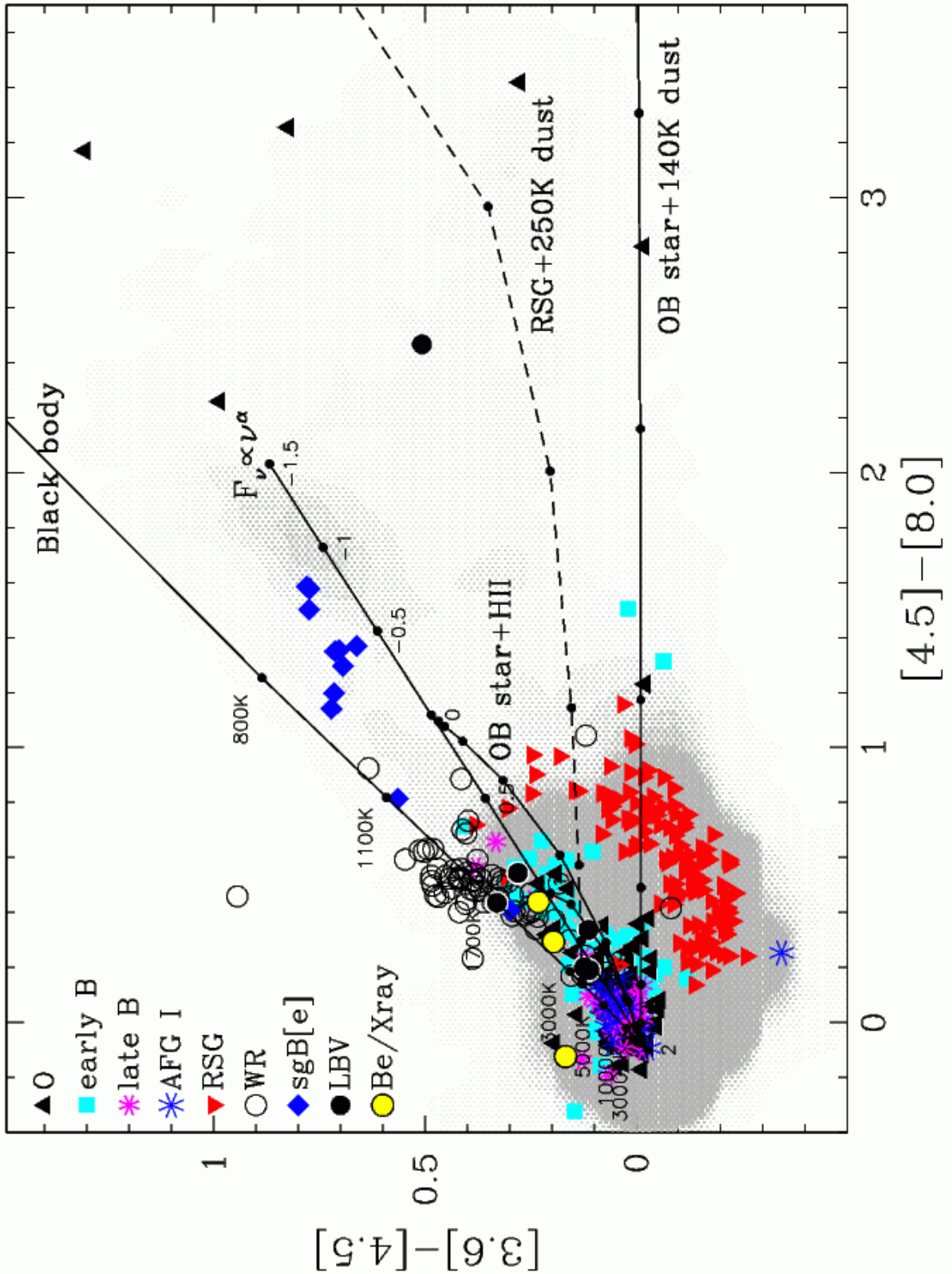


Fig. 7.— Same as Figure 6, but for the $[3.6] - [4.5]$ vs. $[4.5] - [8.0]$ diagram. The majority of hot massive stars lie between the blackbody and OB star +wind model, illustrating that a BB is a good approximation in the infrared.

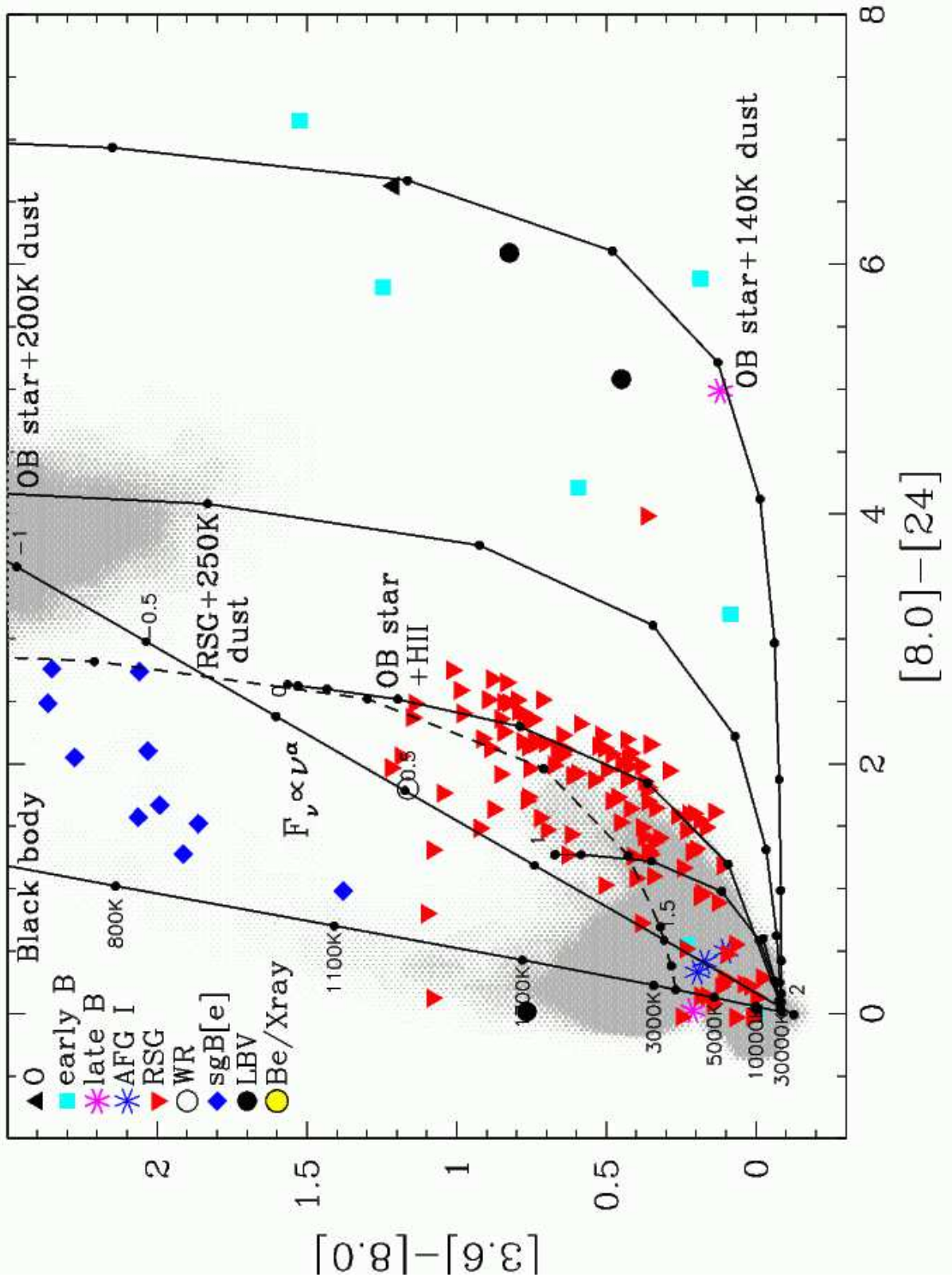


Fig. 8.— Same as Figure 6, but for the $[3.6] - [8.0]$ vs. $[8.0] - [24]$ diagram. The RSG with “bluer” colors have earlier spectral types, indicating a temperature sequence (see §9).

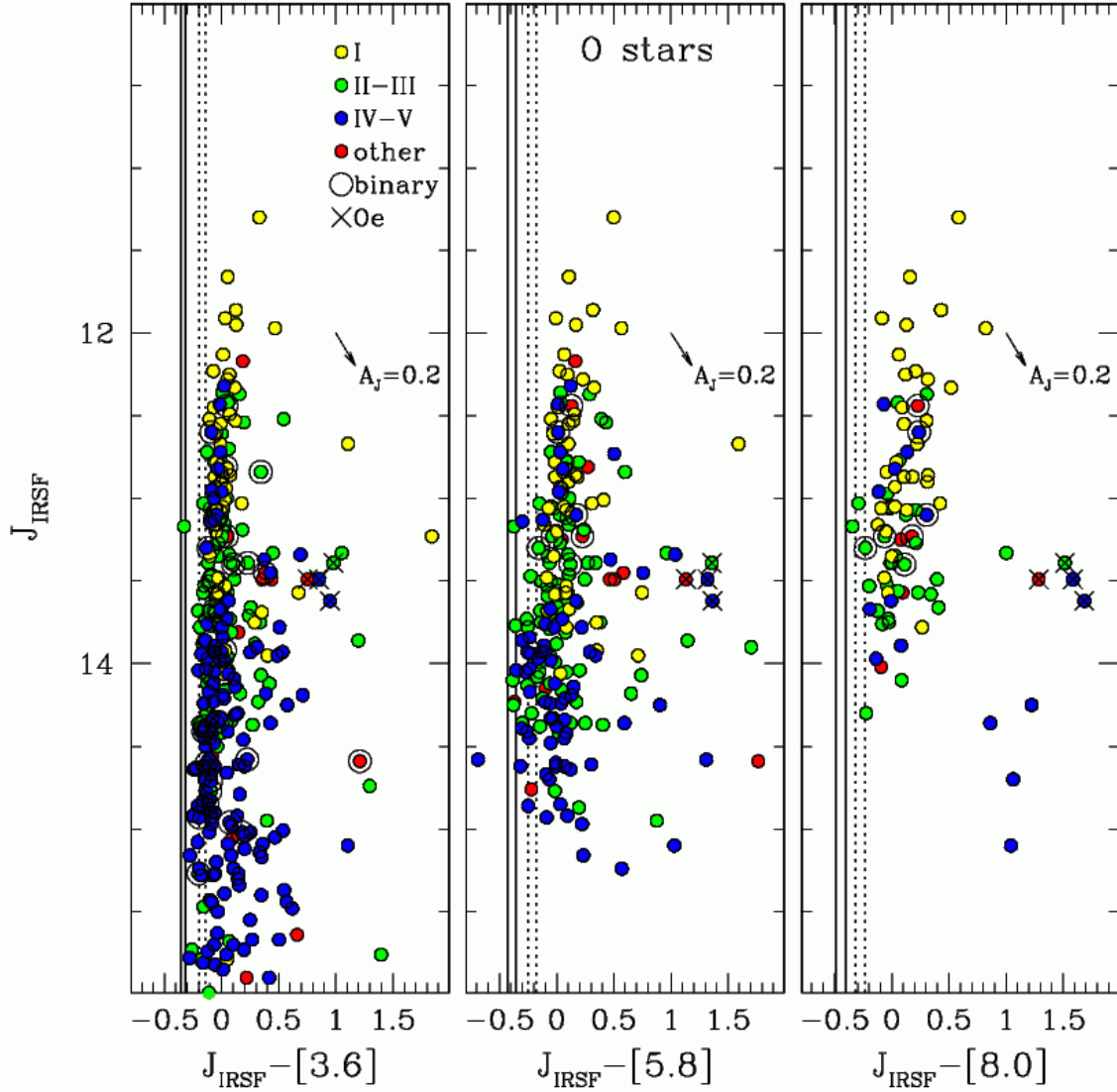


Fig. 9.— Infrared excesses (J_{IRSF} vs. $J_{\text{IRSF}} - [3.6]$, $J_{\text{IRSF}} - [5.8]$ and $J_{\text{IRSF}} - [8.0]$) for 354 O stars. Supergiants are shown in yellow, giants in green, main-sequence stars in blue, stars with uncertain classifications (“other”) in red, binaries with a large circle and Oe stars with an \times . The solid lines correspond to 30kK and 50kK TLUSTY models with $\log g = 4.0$. A reddening vector for $E(B - V) = 0.2$ mag is shown, as well as reddened TLUSTY models by this same amount (dotted lines). The more luminous stars exhibit larger infrared excesses, which increase with λ . The 0.2 – 0.4 mag spread in excesses at any J_{IRSF} -band magnitude reflects the range in mass-loss rates, terminal velocities, clumping properties and, perhaps, rotation rates of O stars.

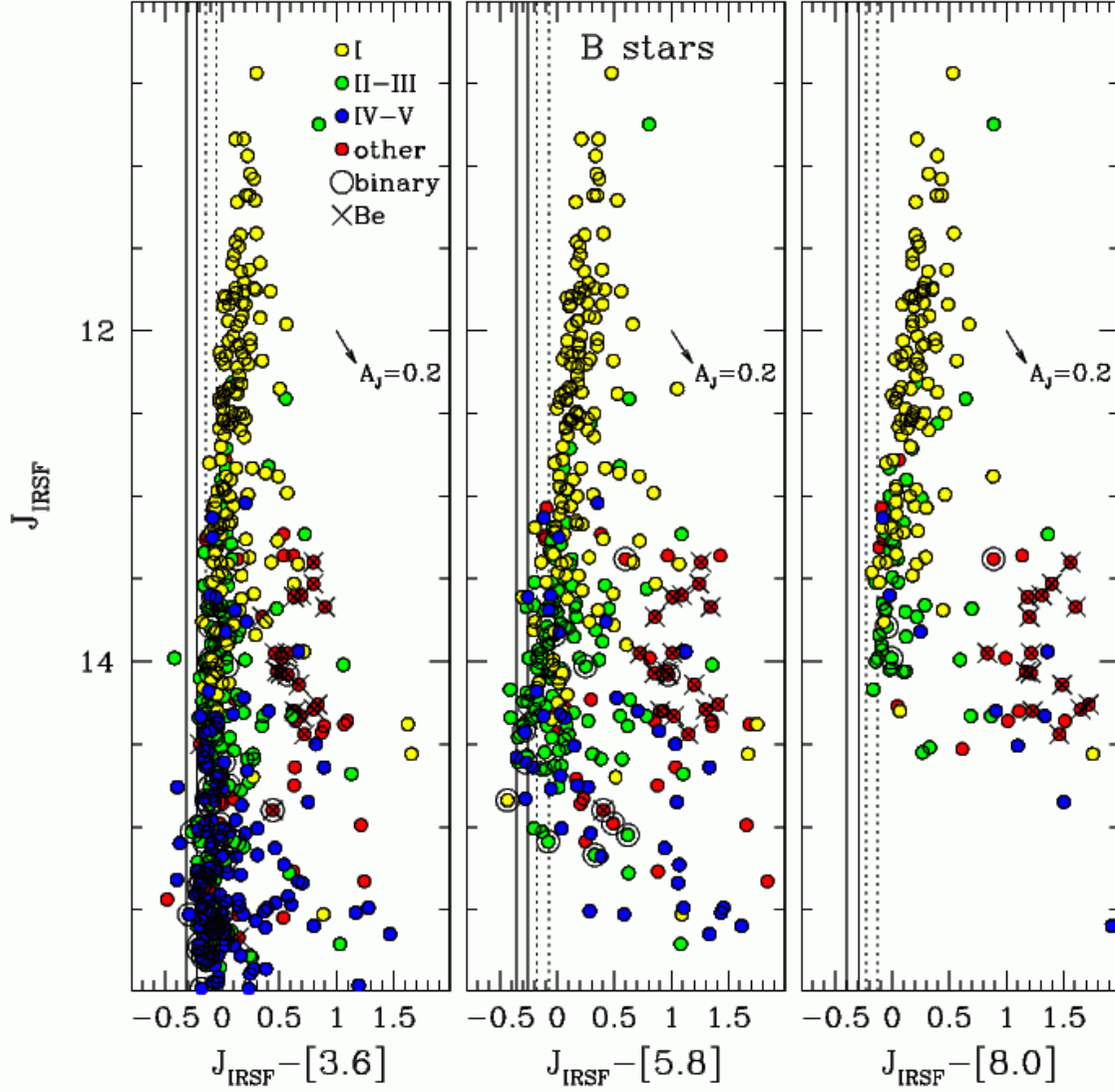


Fig. 10.— Same as Figure 9, but for 586 early-B stars. The solid lines correspond to 20kK, $\log g = 3.0$ and 30kK, $\log g = 4.0$ TLUSTY models. A reddening vector for $E(B - V) = 0.2$ mag is shown, as well as reddened TLUSTY models by this same amount (dotted lines). The larger number of early-B stars makes the trends identified among the O stars clearer.

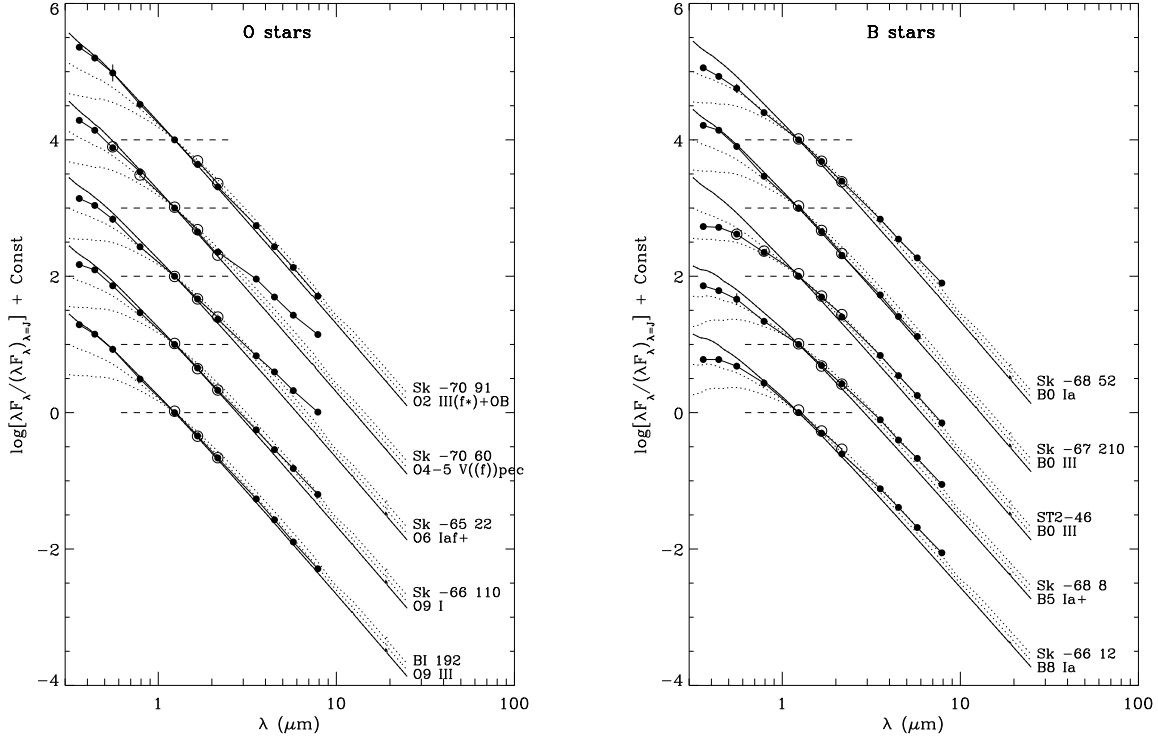


Fig. 11.— Representative SEDs of O stars (*Left*) and B stars (*Right*), normalized by their J -band fluxes (dashed line) and offset for display purposes. Normalized TLUSTY model atmospheres (30kK, $\log g = 3.0$ model for the O and B0 stars; 15kK, $\log g = 1.75$ model for the late B stars) are overplotted for comparison. The MCPS, IRSF and SAGE measurements are shown as filled circles; the 2MASS and OGLE measurements as open circles. The dotted curves correspond to TLUSTY models reddened by $E(B - V) = 0.25$ and 0.50 mag. Infrared excesses are detected in most stars (see §5.1).

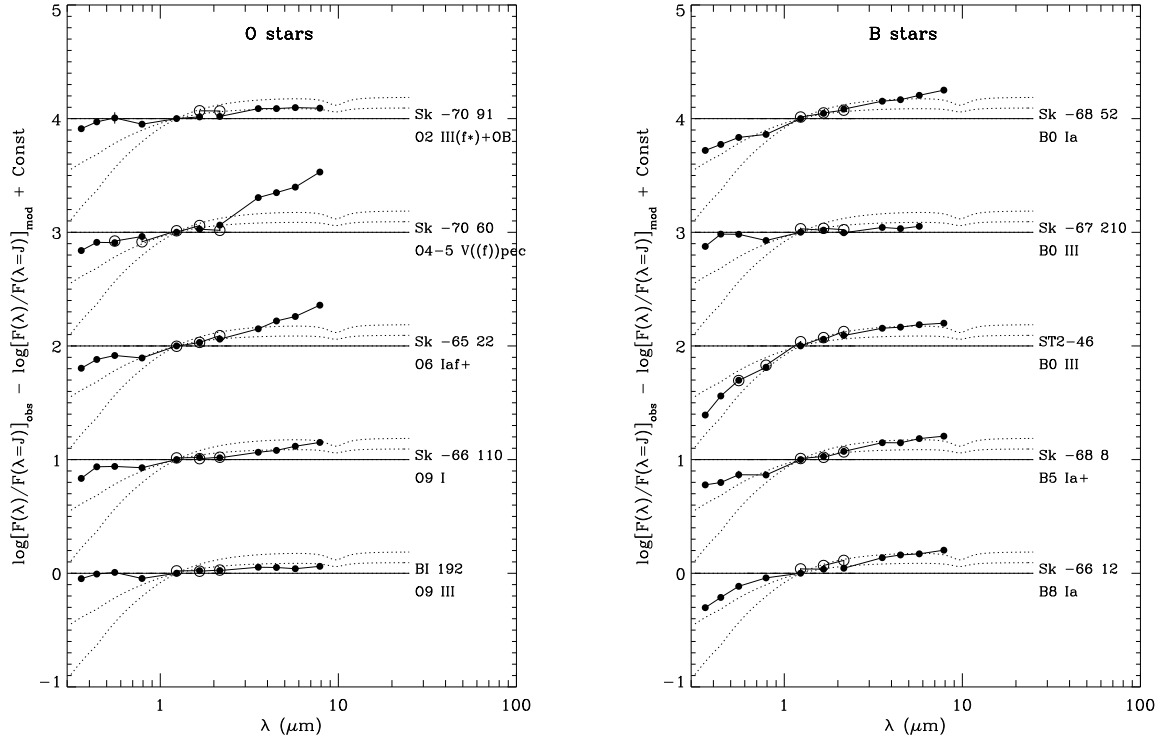


Fig. 12.— Ratios of the SEDs of O stars (*Left*) and B stars (*Right*) to the unreddened TLUSTY models shown in Figure 11, clearly showing the deviations of the observations from the models and cases of variability, from a comparison of $VIJHK_s$ magnitudes obtained from different sources. Dotted curves correspond to TLUSTY models reddened by $E(B - V) = 0.25$ and 0.50 mag. Infrared excesses are present in most cases.

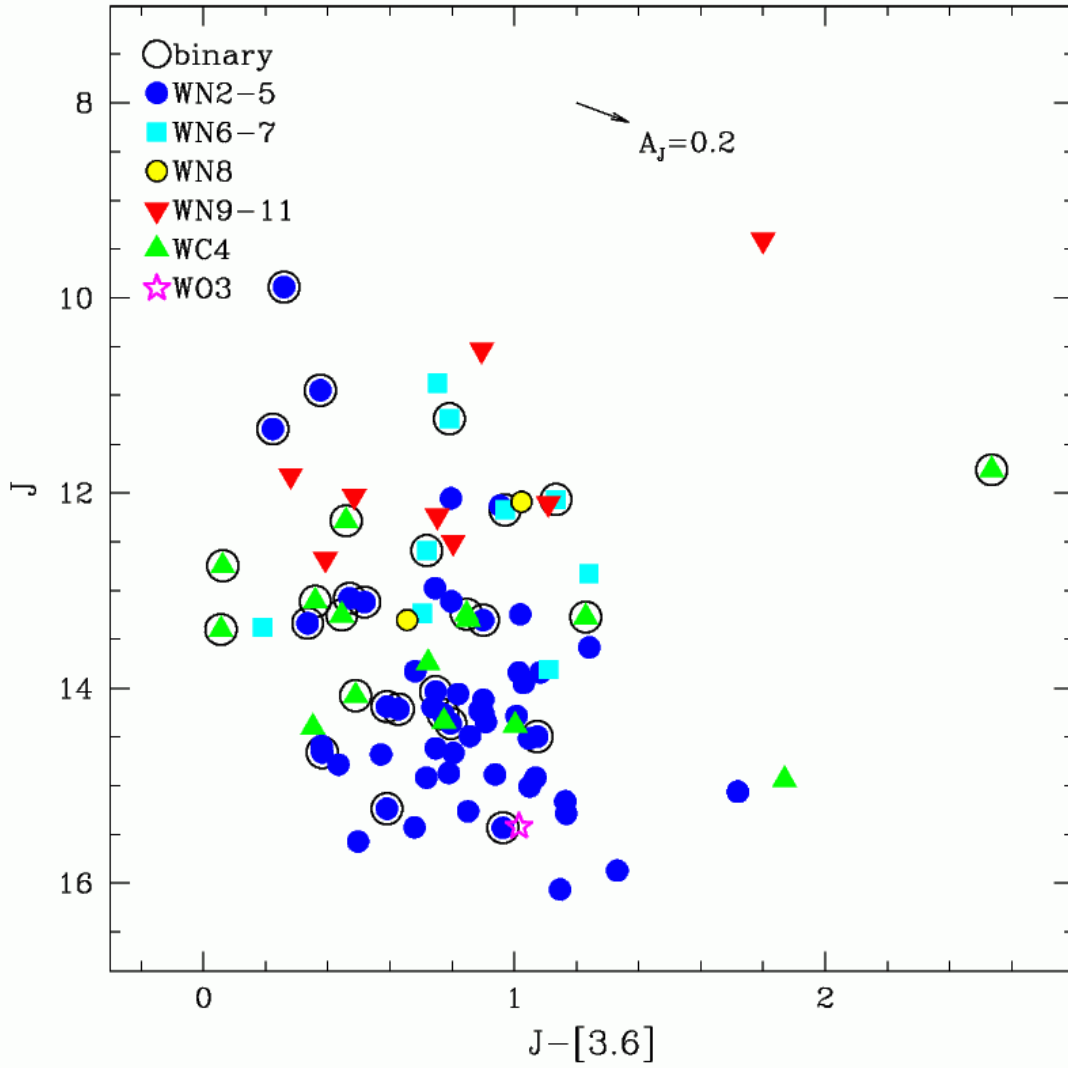


Fig. 13.— J vs. $J - [3.6]$ color magnitude diagram for Wolf-Rayet stars with infrared detections, labelled according to spectral type. Black circles denote known binaries. The reddening vector for $E(B - V) = 0.2$ mag is shown. The WN2-5 stars are on average fainter, while the WN6-7 and WN9-11 are brighter at J -band.

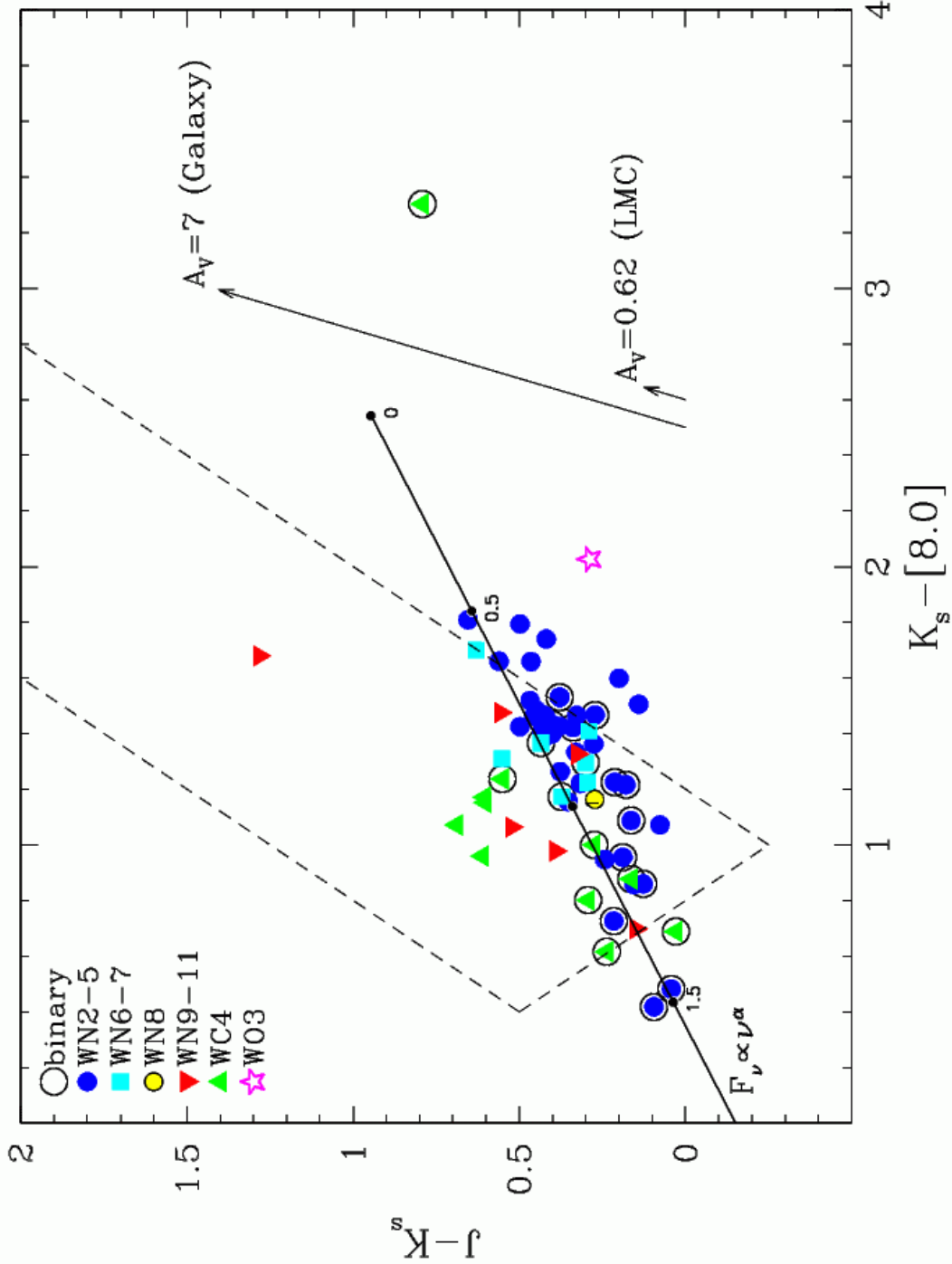


Fig. 14.— $J - K_s$ vs. $K_s - [8.0]$ diagram for Wolf-Rayet stars with infrared detections, showing a tight linear correlation independent of spectral type. The dashed lines correspond to the colors found by Hadfield et al. (2007) for Galactic WR stars; the solid line shows a power law model $F_\nu \propto \nu^\alpha$, for $0 \leq \alpha < 2$. The difference in colors between the LMC WR stars and the Galactic WR stars is a combination of extinction, as illustrated by the reddening vectors, and the large fraction of dusty WC9 stars among Galactic WR stars.

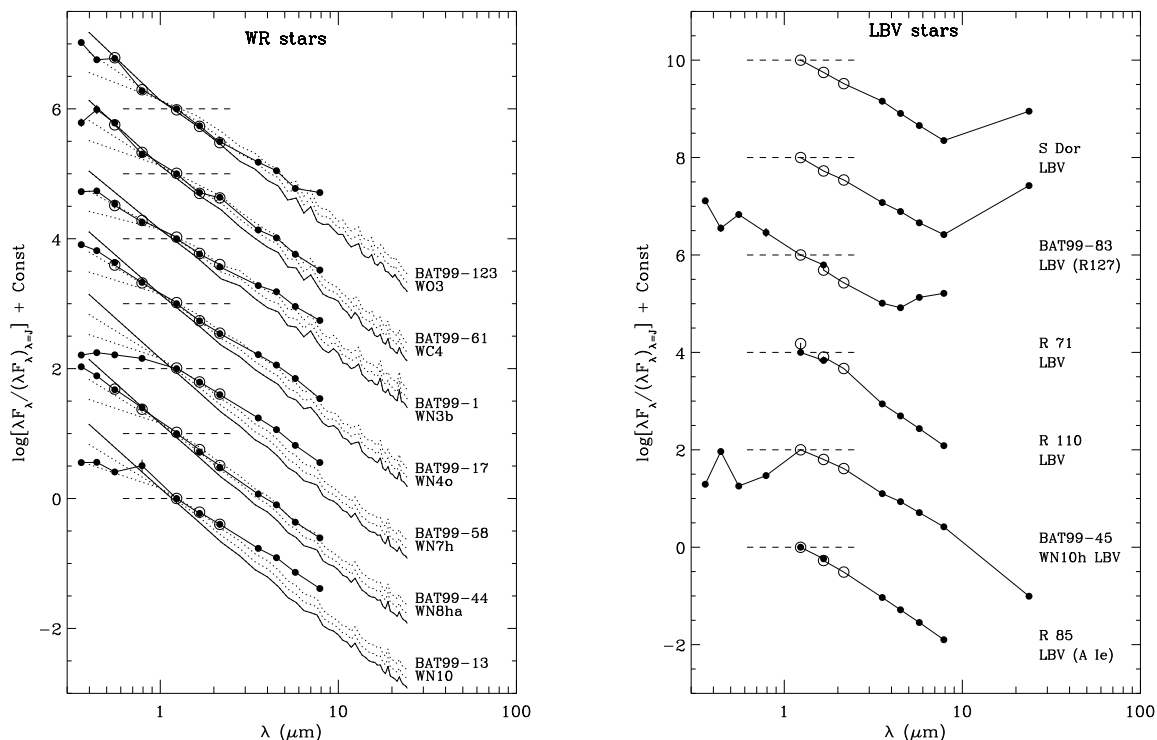


Fig. 15.— Same as Figure 11, but for Wolf-Rayet stars (*Left*) and Luminous Blue Variables (*Right*). For the WR stars, we show model fits for BAT99-123, BAT99-61 and BAT99-17 and generic CMFGEN models for the rest (see §6). All show excess above that predicted by the models. The first 3 LBVs show evidence for dust; BAT99-83 and R71 (saturated at [24]) were detected in the MIPS70 band. The different shapes of the LBV SEDs are likely related to the time since the last outburst event and the amount of dust formed.

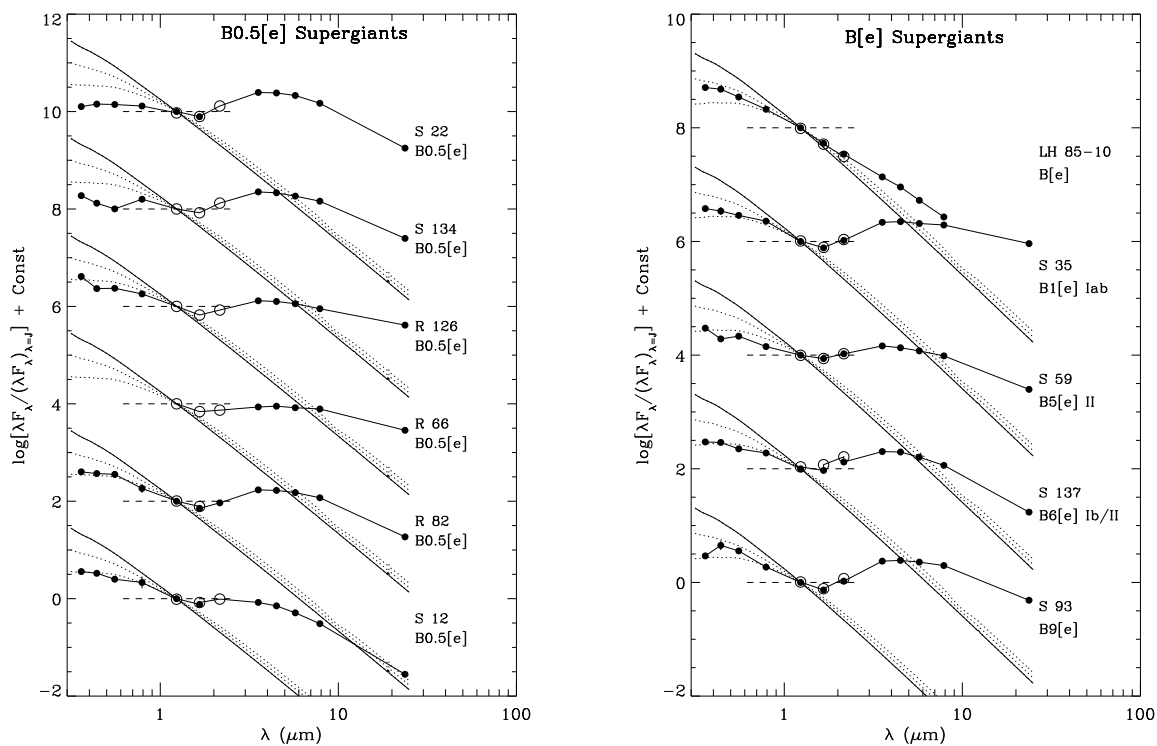


Fig. 16.— Same as Figure 11, but for B[e] supergiants, with a 20kK, $\log g = 2.25$ TLUSTY model overplotted. The sgB[e] have similar SEDs revealing dust, except for LH 85-10, which has a SED similar to that of a Be star. R126, R66, and S35 were also detected in the MIPS70 band (see §8).

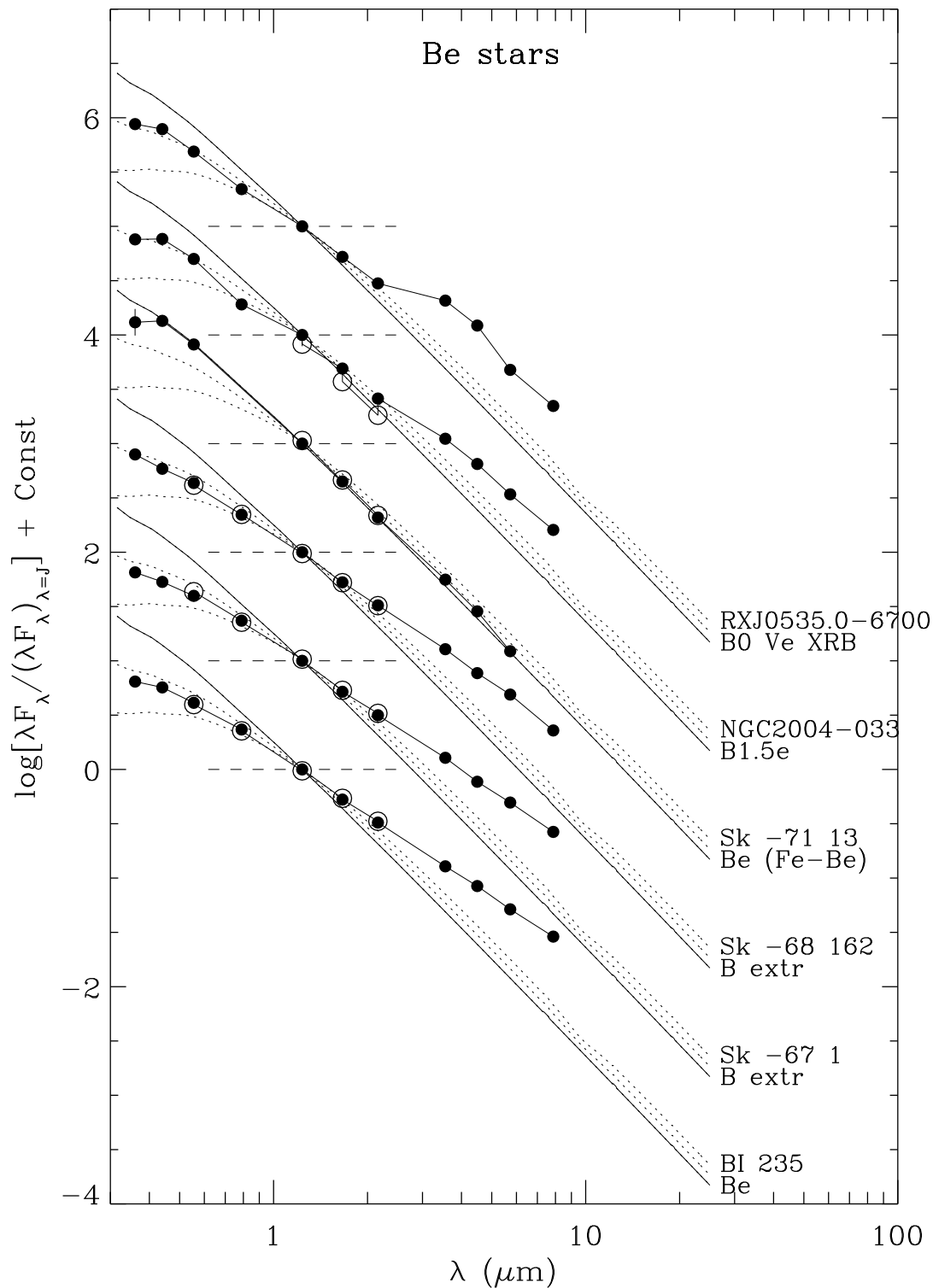


Fig. 17.— Same as Figure 11, but for classical Be stars, with a 25kK, $\log g = 2.75$ TLUSTY model overplotted. The similarity of their SEDs implies that the various spectral types refer to the same type of object. The Be/X-ray binary RXJ0535.0-6700 exhibits excess emission

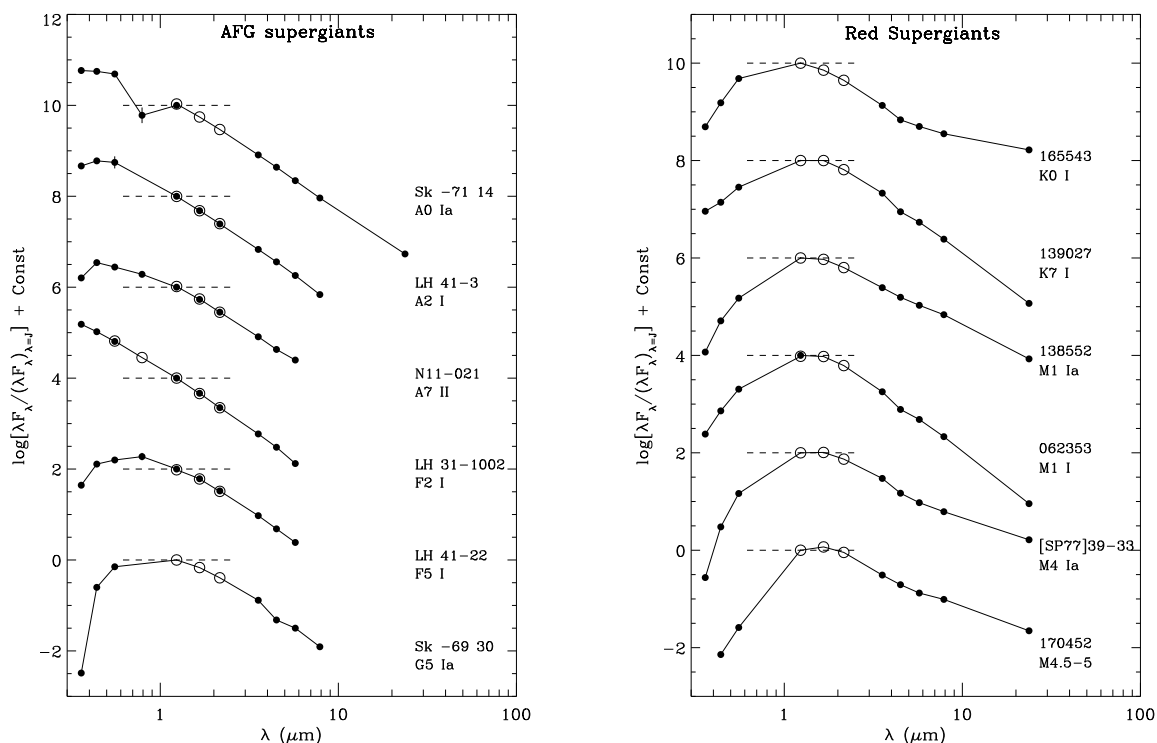


Fig. 18.— Same as Figure 11, but for A, F and G supergiants (*Left*) and K and M supergiants (*Right*). No reference models are shown. The SED of LH 31-1002 (F2 I) implies a hot effective temperature, inconsistent with its spectral type. The K7 I star 139027 has an excess at the shortest wavelengths, possibly indicating a hot companion. The M4.5-5 supergiant 170452 is a rare case of a RSG that changed spectral type (see §9).

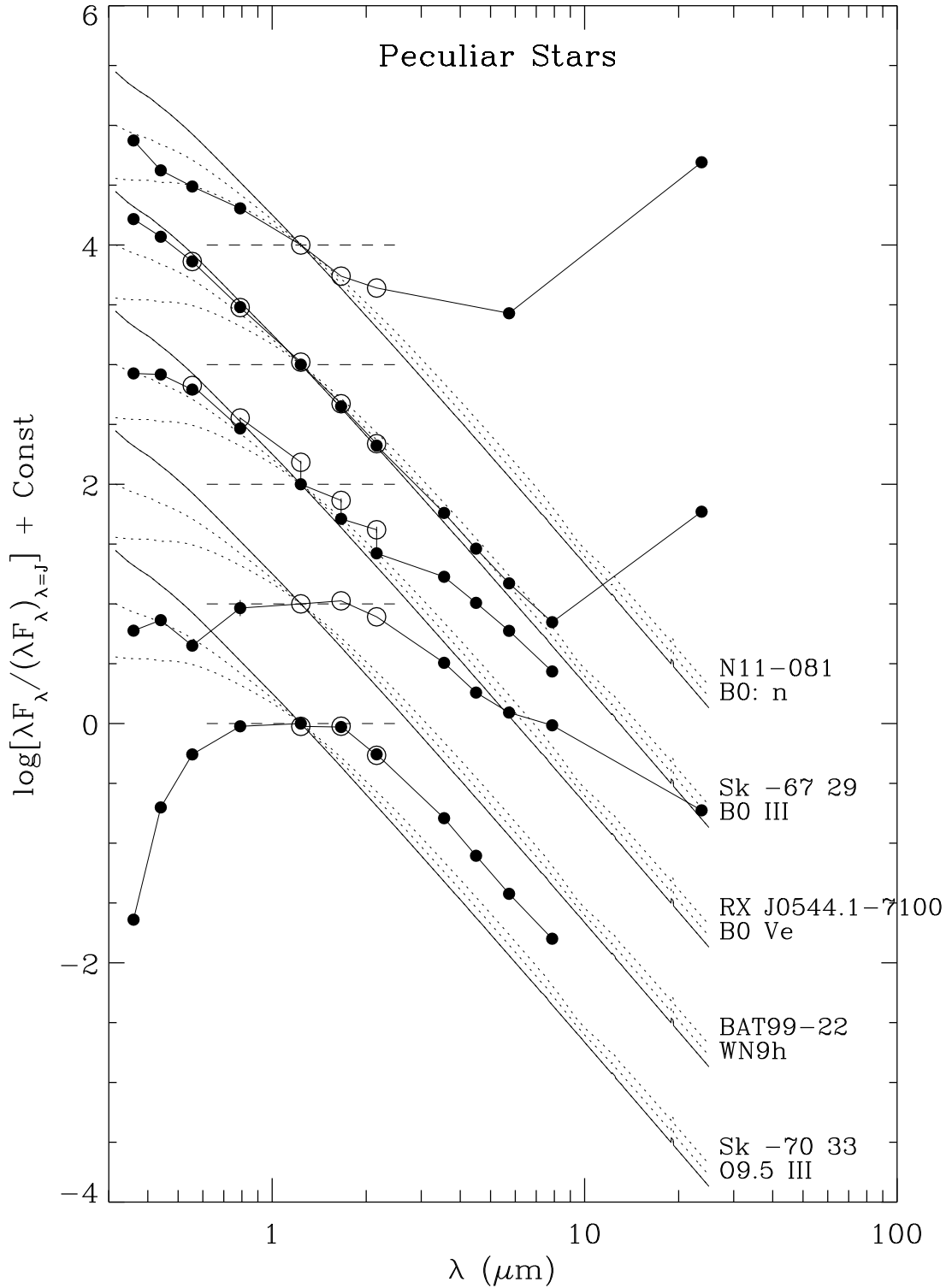


Fig. 19.— Same as Figure 11, but for peculiar SEDs, arising from nebular contamination (N11-081), variability (RXJ0544.1-7100), blending (BAT99-22) or misidentification at one (Sk -67° 29; at 24 μm), or all (Sk -70° 33) bands.

REFERENCES

- Abbott, D. C., Beiging, J. H., Churchwell, E., et al. 1986, *ApJ*, 303, 239
- Abbott, D. C., Bieging, J. H., & Churchwell, E. 1981, *ApJ*, 250, 645
- Abbott, D. C., Telesco, C. M., & Wolff, S. C. 1984, *ApJ*, 279, 225
- Barlow, M. J., Smith, L. J., & Willis, A. J. 1981, *MNRAS*, 196, 101
- Barniske, A., Oskinova, L. M., & Hamann, W.-R. 2008, *A&A*, 486, 971
- Bartzakos, P., Moffat, A. F. J., & Niemela, V. S. 2001, *MNRAS*, 324, 18
- Berger, E., Soderberg, A. M., Chevalier, R. A., et al. 2009, *ApJ*, 699, 1850
- Bertout, C., Leitherer, C., Stahl, O., & Wolf, B. 1985, *A&A*, 144, 87
- Bessell, M. S., Castelli, F., & Plez, B. 1998, *A&A*, 333, 231
- Blomme, R., van de Steene, G. C., Prinja, R. K., et al. 2003, *A&A*, 408, 715
- Blum, R. D., Mould, J. R., Olsen, K. A., et al. 2006, *AJ*, 132, 2034
- Bohannon, B. & Walborn, N. R. 1989, *PASP*, 101, 520
- Bolatto, A. D., Simon, J. D., Stanimirović, S., et al. 2007, *ApJ*, 655, 212
- Bonanos, A. Z. 2009, *ApJ*, 691, 407
- Bonanos, A. Z., Stanek, K. Z., Kudritzki, R. P., et al. 2006, *ApJ*, 652, 313
- Bond, H. E., Bedin, L. R., Bonanos, A. Z., et al. 2009, *ApJ*, 695, L154
- Boyer, M. L., Skillman, E. D., van Loon, J. T., et al. 2009, *ApJ*, 697, 1993
- Breysacher, J., Azzopardi, M., & Testor, G. 1999, *A&AS*, 137, 117
- Brunet, J. P., Imbert, M., Martin, N., et al. 1975, *A&AS*, 21, 109
- Buchanan, C. L., Kastner, J. H., Forrest, W. J., et al. 2006, *AJ*, 132, 1890
- Cannon, J. M., Walter, F., Armus, L., et al. 2006, *ApJ*, 652, 1170
- Castor, J. I. & Simon, T. 1983, *ApJ*, 265, 304
- Clark, J. S., Negueruela, I., Crowther, P. A., et al. 2005, *A&A*, 434, 949

- Conti, P. S., Garmany, C. D., & Massey, P. 1986, *AJ*, 92, 48
- Crowther, P. A. 2006, in *Astronomical Society of the Pacific Conference Series*, Vol. 353, *Stellar Evolution at Low Metallicity: Mass Loss, Explosions, Cosmology*, ed. H. J. G. L. M. Lamers, N. Langer, T. Nugis, & K. Annuk, 157–+
- Crowther, P. A. 2007, *ARA&A*, 45, 177
- Crowther, P. A., Dessart, L., Hillier, D. J., et al. 2002, *A&A*, 392, 653
- Crowther, P. A., Fullerton, A. W., Hillier, D. J., et al. 2000, *ApJ*, 538, L51
- Cutri, R. M. et al. 2004, in *Bulletin of the American Astronomical Society*, Vol. 36, *Bulletin of the American Astronomical Society*, 1487–+
- De Becker, M. 2007, *A&A Rev.*, 14, 171
- Dopita, M. A., Bell, J. F., Chu, Y.-H., et al. 1994, *ApJS*, 93, 455
- Evans, C. J., Lennon, D. J., Smartt, S. J., et al. 2006, *A&A*, 456, 623
- Faccioli, L., Alcock, C., Cook, K., et al. 2007, *AJ*, 134, 1963
- Fazio, G. G., Hora, J. L., Allen, L. E., et al. 2004, *ApJS*, 154, 10
- Fitzpatrick, E. L. 1988, *ApJ*, 335, 703
- . 1991, *PASP*, 103, 1123
- Fitzpatrick, E. L. & Massa, D. 2009, *ApJ*, 699, 1209
- Fitzpatrick, E. L., Ribas, I., Guinan, E. F., et al. 2002, *ApJ*, 564, 260
- . 2003, *ApJ*, 587, 685
- Foellmi, C., Moffat, A. F. J., & Guerrero, M. A. 2003, *MNRAS*, 338, 1025
- Fullerton, A. W., Crowther, P. A., De Marco, O., et al. 2000, *ApJ*, 538, L43
- Garcia, M., Herrero, A., Vicente, B., et al. 2009, *A&A* in press (arXiv:0904.4455)
- Garmany, C. D. & Humphreys, R. M. 1985, *AJ*, 90, 2009
- Garmany, C. D., Massey, P., & Parker, J. W. 1994, *AJ*, 108, 1256
- Gehrz, R. D. & Hackwell, J. A. 1974, *ApJ*, 194, 619

- Gehrz, R. D., Hackwell, J. A., & Jones, T. W. 1974, *ApJ*, 191, 675
- González, J. F., Ostrov, P., Morrell, N., & Minniti, D. 2005, *ApJ*, 624, 946
- Guinan, E. F., Fitzpatrick, E. L., Dewarf, L. E., et al. 1998, *ApJ*, 509, L21
- Hadfield, L. J., van Dyk, S. D., Morris, P. W., et al. 2007, *MNRAS*, 376, 248
- Henize, K. G. 1956, *ApJS*, 2, 315
- Heydari-Malayeri, M., Courbin, F., Rauw, G., et al. 1997, *A&A*, 326, 143
- Heydari-Malayeri, M. & Melnick, J. 1992, *A&A*, 258, L13
- Heydari-Malayeri, M., Meynadier, F., & Walborn, N. R. 2003, *A&A*, 400, 923
- Hillier, D. J. & Miller, D. L. 1998, *ApJ*, 496, 407
- Hora, J. L., Cohen, M., Ellis, R. G., et al. 2008, *AJ*, 135, 726
- Humphreys, R. M. 1979, *ApJS*, 39, 389
- Humphreys, R. M. & Davidson, K. 1979, *ApJ*, 232, 409
- . 1994, *PASP*, 106, 1025
- Jackson, D. C., Skillman, E. D., Gehrz, R. D., et al. 2007a, *ApJ*, 656, 818
- . 2007b, *ApJ*, 667, 891
- Jaxon, E. G., Guerrero, M. A., Howk, J. C., et al. 2001, *PASP*, 113, 1130
- Josselin, E., Blommaert, J. A. D. L., Groenewegen, M. A. T., et al. 2000, *A&A*, 357, 225
- Kastner, J. H., Buchanan, C. L., Sargent, B., et al. 2006, *ApJ*, 638, L29
- Kato, D., Nagashima, C., Nagayama, T., et al. 2007, *PASJ*, 59, 615
- Koornneef, J. 1983, *A&A*, 128, 84
- Kraus, M., Borges Fernandes, M., & de Araújo, F. X. 2007, *A&A*, 463, 627
- Lamers, H. J. G. L. M. & Leitherer, C. 1993, *ApJ*, 412, 771
- Lamers, H. J. G. L. M., Zickgraf, F.-J., de Winter, D., et al. 1998, *A&A*, 340, 117

- Langer, N. & Heger, A. 1998, in *Astrophysics and Space Science Library*, Vol. 233, B[e] stars, ed. A. M. Hubert & C. Jaschek, 235–+
- Lanz, T. & Hubeny, I. 2003, *ApJS*, 146, 417
- . 2007, *ApJS*, 169, 83
- Leitherer, C. & Wolf, B. 1984, *A&A*, 132, 151
- Lennon, D. J., Wobig, D., Kudritzki, R.-P., et al. 1993, *Space Science Reviews*, 66, 207
- Levesque, E. M., Massey, P., Olsen, K. A. G., et al. 2007, *ApJ*, 667, 202
- Liu, Q. Z., van Paradijs, J., & van den Heuvel, E. P. J. 2005, *A&A*, 442, 1135
- Lucke, P. B. 1972, PhD thesis, AA(UNIVERSITY OF WASHINGTON.)
- Macri, L. M., Stanek, K. Z., Bersier, D., et al. 2006, *ApJ*, 652, 1133
- Massa, D., Fullerton, A. W., Sonneborn, G., et al. 2003, *ApJ*, 586, 996
- Massey, P. 2002, *ApJS*, 141, 81
- . 2003, *ARA&A*, 41, 15
- . 2009, (arXiv:0903.0155)
- Massey, P., Bresolin, F., Kudritzki, R. P., et al. 2004, *ApJ*, 608, 1001
- Massey, P., Lang, C. C., Degioia-Eastwood, K., et al. 1995, *ApJ*, 438, 188
- Massey, P. & Olsen, K. A. G. 2003, *AJ*, 126, 2867
- Massey, P., Penny, L. R., & Vukovich, J. 2002, *ApJ*, 565, 982
- Massey, P., Puls, J., Pauldrach, A. W. A., et al. 2005, *ApJ*, 627, 477
- Massey, P., Waterhouse, E., & DeGioia-Eastwood, K. 2000, *AJ*, 119, 2214
- McQuinn, K. B. W., Woodward, C. E., Willner, S. P., et al. 2007, *ApJ*, 664, 850
- Meixner, M., Gordon, K. D., Indebetouw, R., et al. 2006, *AJ*, 132, 2268
- Mennickent, R. E., Cidale, L., Díaz, M., et al. 2005, *MNRAS*, 357, 1219
- Mennickent, R. E., Kołaczowski, Z., Michalska, G., et al. 2008, *MNRAS*, 389, 1605

- Mennickent, R. E., Pietrzyński, G., Diaz, M., et al. 2003, *A&A*, 399, L47
- Meynadier, F., Heydari-Malayeri, M., & Walborn, N. R. 2005, *A&A*, 436, 117
- Meynet, G. & Maeder, A. 2006, in *Astronomical Society of the Pacific Conference Series*, Vol. 355, *Stars with the B[e] Phenomenon*, ed. M. Kraus & A. S. Miroshnichenko, 27–+
- Moffat, A. F. J., Niemela, V. S., & Marraco, H. G. 1990, *ApJ*, 348, 232
- Moffat, A. F. J. & Robert, C. 1994, *ApJ*, 421, 310
- Mokiem, M. R., de Koter, A., Vink, J. S., et al. 2007, *A&A*, 473, 603
- Mould, J., Barmby, P., Gordon, K., et al. 2008, *ApJ*, 687, 230
- Natta, A. & Panagia, N. 1976, *A&A*, 50, 191
- Negueruela, I. 2004, *Astronomische Nachrichten*, 325, 380
- Negueruela, I., Steele, I. A., & Bernabeu, G. 2004, *Astronomische Nachrichten*, 325, 749
- Niemela, V. S. & Bassino, L. P. 1994, *ApJ*, 437, 332
- Niemela, V. S., Seggewiss, W., & Moffat, A. F. J. 2001, *A&A*, 369, 544
- Nikolaev, S., Drake, A. J., Keller, S. C., et al. 2004, *ApJ*, 601, 260
- Nishiyama, S., Tamura, M., Hatano, H., Kato, D., et al. 2009, *ApJ*, 696, 1407
- Oey, M. S. & Massey, P. 1995, *ApJ*, 452, 210
- Olsen, K. A. G., Kim, S., & Buss, J. F. 2001, *AJ*, 121, 3075
- Ostrov, P. G. 2001, *MNRAS*, 321, L25
- Ostrov, P. G. & Lapasset, E. 2003, *MNRAS*, 338, 141
- Ostrov, P. G., Morrell, N. I., & Lapasset, E. 2001, *A&A*, 377, 972
- Owocki, S. P., Cranmer, S. R., & Blondin, J. M. 1994, *ApJ*, 424, 887
- Panagia, N. 1991, in *NATO ASIC Proc. 342: The Physics of Star Formation and Early Stellar Evolution*, ed. C. J. Lada & N. D. Kylafis, 565–+
- Panagia, N. & Felli, M. 1975, *A&A*, 39, 1

- Panagia, N. & Macchetto, F. 1982, *A&A*, 106, 266
- Parker, J. W. 1993, *AJ*, 106, 560
- Parker, J. W., Garmany, C. D., Massey, P., et al. 1992, *AJ*, 103, 1205
- Parker, J. W., Zaritsky, D., Stecher, T. P., et al. 2001, *AJ*, 121, 891
- Pei, Y. C. 1992, *ApJ*, 395, 130
- Podsiadlowski, P., Morris, T. S., & Ivanova, N. 2006, in *Astronomical Society of the Pacific Conference Series*, Vol. 355, *Stars with the B[e] Phenomenon*, ed. M. Kraus & A. S. Miroshnichenko, 259–+
- Pojmanski, G. 2002, *Acta Astronomica*, 52, 397
- Porter, J. M. 2003, *A&A*, 398, 631
- Porter, J. M. & Rivinius, T. 2003, *PASP*, 115, 1153
- Prieto, J. L. 2008, *The Astronomer’s Telegram*, 1550, 1
- Prieto, J. L., Kistler, M. D., Thompson, T. A., et al. 2008, *ApJ*, 681, L9
- Puls, J., Markova, N., Scuderi, S., et al. 2006, *A&A*, 454, 625
- Raguzova, N. V. & Popov, S. B. 2005, *Astronomical and Astrophysical Transactions*, 24, 151
- Reach, W. T., Megeath, S. T., Cohen, M., et al. 2005, *PASP*, 117, 978
- Ribas, I., Fitzpatrick, E. L., Maloney, F. P., et al. 2002, *ApJ*, 574, 771
- Rieke, G. H., Blaylock, M., Decin, L., et al. 2008, *AJ*, 135, 2245
- Rieke, G. H., Rieke, M. J., & Paul, A. E. 1989, *ApJ*, 336, 752
- Rieke, G. H., Young, E. T., Engelbracht, C. W., et al. 2004, *ApJS*, 154, 25
- Rousseau, J., Martin, N., Prévot, L., et al. 1978, *A&AS*, 31, 243
- Sanduleak, N. 1970, *Contributions from the Cerro Tololo Inter-American Observatory*, 89
- . 2008, *VizieR Online Data Catalog*, 3113, 0
- Schild, H. & Testor, G. 1992, *A&AS*, 92, 729
- Schild, R. E. 1966, *ApJ*, 146, 142

- Schnurr, O., Moffat, A. F. J., St-Louis, N., et al. 2008, MNRAS, 389, 806
- Scuderi, S., Panagia, N., Stanghellini, C., et al. 1998, A&A, 332, 251
- Skrutskie, M. F., Cutri, R. M., Stiening, R., et al. 2006, AJ, 131, 1163
- Smith, L. J., Crowther, P. A., & Prinja, R. K. 1994, A&A, 281, 833
- Smith, L. J., Norris, R. P. F., & Crowther, P. A. 2002, MNRAS, 337, 1309
- Smith, N. & Conti, P. S. 2008, ApJ, 679, 1467
- Smith, N., Ganeshalingam, M., Chornock, R., et al. 2009, ApJ, 697, L49
- Snedden, C., Gehrz, R. D., Hackwell, J. A., et al. 1978, ApJ, 223, 168
- Srinivasan, S., Meixner, M., Leitherer, C., et al. 2009, AJ, 137, 4810
- Testor, G. & Niemela, V. 1998, A&AS, 130, 527
- Thompson, T. A., Prieto, J. L., Stanek, K. Z., et al. 2008, in press (arXiv:0809.0510)
- Udalski, A., Soszynski, I., Szymanski, M. K., et al. 2008, Acta Astronomica, 58, 89
- Verhoelst, T., van der Zypen, N., Hony, S., et al. 2009, A&A, 498, 127
- Verley, S., Hunt, L. K., Corbelli, E., et al. 2007, A&A, 476, 1161
- Vijh, U. P., Meixner, M., Babler, B., et al. 2009, AJ, 137, 3139
- Voors, R. H. M., Waters, L. B. F. M., Morris, P. W., et al. 1999, A&A, 341, L67
- Walborn, N. R. 1977, ApJ, 215, 53
- Walborn, N. R. & Blades, J. C. 1997, ApJS, 112, 457
- Walborn, N. R., Fullerton, A. W., Crowther, P. A., et al. 2002, ApJS, 141, 443
- Walborn, N. R., Howarth, I. D., Herrero, A., & Lennon, D. J. 2003, ApJ, 588, 1025
- Walborn, N. R., Morrell, N. I., Howarth, et al. 2004, ApJ, 608, 1028
- Walborn, N. R., Stahl, O., Gamen, R. C., et al. 2008, ApJ, 683, L33
- Wegner, W. 1994, MNRAS, 270, 229
- Weis, K. 2003, A&A, 408, 205

- Westerlund, B. 1961, Uppsala Astronomical Observatory Annals, 5, 1
- Whitney, B. A., Sewilo, M., Indebetouw, R., et al. 2008, AJ, 136, 18
- Williams, S. J., Gies, D. R., Henry, T. J., et al. 2008, ApJ, 682, 492
- Wright, A. E. & Barlow, M. J. 1975, MNRAS, 170, 41
- Wright, K. O. 1970, Vistas in Astronomy, 12, 147
- Wyrzykowski, L., Udalski, A., Kubiak, M., et al. 2003, Acta Astronomica, 53, 1
- Zaritsky, D., Harris, J., Thompson, I. B., et al. 2004, AJ, 128, 1606
- Zickgraf, F.-J. 2006, in Astronomical Society of the Pacific Conference Series, Vol. 355, Stars with the B[e] Phenomenon, ed. M. Kraus & A. S. Miroshnichenko, 135–+
- Zickgraf, F.-J., Wolf, B., Leitherer, C., et al. 1986, A&A, 163, 119
- Zsargó, J., Hillier, D. J., & Georgiev, L. N. 2008, A&A, 478, 543

Table 1. CATALOG OF SPECTRAL TYPES FOR 1750 LMC MASSIVE STARS

Star Name ^a	RA (J2000) (deg)	Dec (J2000) (deg)	Reference ^b	Classification & Comments
BAT99–1	71.3843765	–70.2530289	F03	WN3b Sk –70 1
Sk –69 1	71.3865433	–69.4670029	C86	B1 III
Sk –67 1	71.4227524	–67.5705261	C86	B extr
Sk –67 2	71.7685394	–67.1147461	F88	B1 Ia+
Sk –70 1a	71.8649979	–70.5626984	C86	O9 II
Sk –69 8	72.3293762	–69.4318314	F88	B5 Ia
BAT99–2	72.4009000	–69.3484000	F03	WN2b(h)
Sk –69 9	72.4642105	–69.2011948	J01	O6.5 III

^aStar designations: Breysacher et al. (BAT99; 1999), Sanduleak (Sk; 1970), Westerlund (W; 1961), Brunet et al. (BI; 1975), Lucke (LH; 1972), Henize (S; 1956)

^bReference key: (B01) Bartzakos et al. (2001), (B09) Bonanos (2009), (C86) Conti et al. (1986), (E06) Evans et al. (2006), (F88) Fitzpatrick (1988, 1991), (F02) Fitzpatrick et al. (2002), (F03a) Fitzpatrick et al. (2003), (F03) Foellmi et al. (2003), (G94) Garmany et al. (1994), (G05) González et al. (2005), (G98) Guinan et al. (1998), (H92) Heydari-Malayeri & Melnick (1992), (H03) Heydari-Malayeri et al. (2003), (H79) Humphreys (1979), (H94) Humphreys & Davidson (1994), (J01) Jaxon et al. (2001), (L05) Liu et al. (2005), (M95) Massey et al. (1995), (M00) Massey et al. (2000), (M02) Massey (2002), (M02b) Massey et al. (2002), (M03) Massey (2003), (M04) Massey et al. (2004), (M05) Massey et al. (2005), (M09) Massey (2009), (Me05) Meynadier et al. (2005), (N94) Niemela & Bassino (1994), (N01) Niemela et al. (2001), (O95) Oey & Massey (1995), (O01) Olsen et al. (2001), (O01b) Ostrov et al. (2001), (O01c) Ostrov (2001), (O03) Ostrov & Lapasset (2003), (P01) Parker et al. (2001), (P92) Parker et al. (1992), (P93) Parker (1993), (R02) Ribas et al. (2002), (R05) Raguzova & Popov (2005), (S92) Schild & Testor (1992), (S08) Schnurr et al. (2008), (T98) Testor & Niemela (1998), (W77) Walborn (1977), (W97) Walborn & Blades (1997), (W02) Walborn et al. (2002), (W03) Walborn et al. (2003), (W04) Walborn et al. (2004), (W08) Williams et al. (2008), (Z06) Zickgraf (2006).

Note. — Table 1 is available in its entirety in the electronic version of the Journal. A portion is shown here for guidance regarding its form and content.

Table 2. STATISTICS FOR THE 1268 MATCHED STARS

Catalogs Matched	# Stars
IRACC	5
IRACC+IRSF	88
IRACC+IRSF+MCPS	601
IRACC+IRSF+MCPS+MIPS24	122
IRACC+IRSF+MCPS+MIPS24+OGLE	9
IRACC+IRSF+MCPS+OGLE	364
IRACC+IRSF+MIPS24	21
IRACC+IRSF+OGLE	18
IRACC+MCPS	33
IRACC+MCPS+MIPS24	1
IRACA+MIPS24	1
IRACA+MCPS+MIPS24	1
IRACCEP1+MCPS+MIPS24	4

Table 3. 0.3-24 μm PHOTOMETRY OF 1268 MASSIVE STARS IN THE LMC

Star Name ^a	IRAC Designation	RA(J2000)	Dec(J2000)	U	σ_U	B	σ_B	...	Ref. ^b	Classification & Comments
BAT99-1	J044532.25-701510.8	71.3843765	-70.2530289	15.001	0.037	15.647	0.029	...	F03	WN3b Sk -70 1
Sk -69 1	J044532.76-692801.2	71.3865433	-69.4670029	12.343	0.01	13.364	0.01	...	C86	B1 III
Sk -67 1	J044541.44-673413.9	71.4227524	-67.5705261	12.829	0.038	13.72	0.025	...	C86	B extr
Sk -67 2	J044704.44-670653.1	71.7685394	-67.1147461	10.351	0.104	11.219	0.095	...	F88	B1 Ia+
Sk -70 1a	J044727.58-703345.6	71.8649979	-70.5626984	12.693	0.01	13.654	0.01	...	C86	O9 II
Sk -69 8	J044919.03-692554.6	72.3293762	-69.4318314	10.838	0.06	11.714	0.078	...	F88	B5 Ia
BAT99-2	J044936.24-692054.8	72.4009	-69.3484	15.633	0.038	16.495	0.03	...	F03	WN2b(h)

^aStar designations: Breysacher et al. (BAT99; 1999), Sanduleak (Sk; 1970), Westerlund (W; 1961), Brunet et al. (BI; 1975), Lucke (LH; 1972), Henize (S; 1956)

^bReference key: (B01) Bartzakos et al. (2001), (B09) Bonanos (2009), (C86) Conti et al. (1986), (E06) Evans et al. (2006), (F88) Fitzpatrick (1988, 1991), (F02) Fitzpatrick et al. (2002), (F03a) Fitzpatrick et al. (2003), (F03) Foellmi et al. (2003), (G94) Garmany et al. (1994), (G05) González et al. (2005), (G98) Guinan et al. (1998), (H92) Heydari-Malayeri & Melnick (1992), (H03) Heydari-Malayeri et al. (2003), (H79) Humphreys (1979), (H94) Humphreys & Davidson (1994), (J01) Jaxon et al. (2001), (L05) Liu et al. (2005), (M95) Massey et al. (1995), (M00) Massey et al. (2000), (M02) Massey (2002), (M02b) Massey et al. (2002), (M03) Massey (2003), (M04) Massey et al. (2004), (M05) Massey et al. (2005), (M09) Massey (2009), (Me05) Meynadier et al. (2005), (N94) Niemela & Bassino (1994), (N01) Niemela et al. (2001), (O95) Oey & Massey (1995), (O01) Olsen et al. (2001), (O01b) Ostrov et al. (2001), (O01c) Ostrov (2001), (O03) Ostrov & Lapasset (2003), (P01) Parker et al. (2001), (P92) Parker et al. (1992), (P93) Parker (1993), (R02) Ribas et al. (2002), (R05) Raguzova & Popov (2005), (S92) Schild & Testor (1992), (S08) Schnurr et al. (2008), (T98) Testor & Niemela (1998), (W77) Walborn (1977), (W97) Walborn & Blades (1997), (W02) Walborn et al. (2002), (W03) Walborn et al. (2003), (W04) Walborn et al. (2004), (W08) Williams et al. (2008), (Z06) Zickgraf (2006).

Note. — Table 3 is available in its entirety in the electronic version of the Journal. A portion is shown here for guidance regarding its form and content.

Table 4. FILTER & DETECTION CHARACTERISTICS

Filter	λ_{eff} (μm)	Zero mag flux (Jy)	Resolution ($''$)	# stars detected
<i>U</i>	0.36	1790	1.5/2.6	1121
<i>B</i>	0.44	4063	1.5/2.6	1136
<i>V</i>	0.555	3636	1.5/2.6	1136
<i>I</i>	0.79	2416	1.5/2.6	1026
<i>V_{OGLE}</i>	0.555	3636	1.2	391
<i>I_{OGLE}</i>	0.79	2416	1.2	391
<i>J</i>	1.235	1594	2.5	1203
<i>H</i>	1.662	1024	2.5	1218
<i>K_s</i>	2.159	666.7	2.5	1184
<i>J_{IRSF}</i>	1.235	1594	1.3	1122
<i>H_{IRSF}</i>	1.662	1024	1.3	1089
<i>K_{sIRSF}</i>	2.159	666.7	1.3	1077
[3.6]	3.55	280.9	1.7	1260
[4.5]	4.493	179.7	1.7	1234
[5.8]	5.731	115.0	1.9	950
[8.0]	7.872	64.13	2	577
[24]	23.68	7.15	6	159

Table 5. MIPS70+160 PHOTOMETRY

Star Name	Spectral Type	mag ₇₀ (mag)	σ_{mag70} (mag)	Flux ₇₀ (mJy)	σ_{Flux70} (mJy)	mag ₁₆₀ (mag)	σ_{mag160} (mag)	Flux ₁₆₀ (mJy)	$\sigma_{Flux160}$ (mJy)
BAT99-8	WC4	1.379	0.02796	218.4	5.623
BAT99-22	WN9h (+RSG)	2.327	0.04657	91.24	3.911
BAT99-32	WN6(h)	1.4	0.03326	214.4	6.564
BAT99-37	WN3o	1.503	0.02847	194.8	5.107
BAT99-38	WC4+[O8I:]	-0.8254	0.01853	1664	28.4	-2.412	0.1344	1476	181.8
BAT99-53	WC4 (+OB)	1.386	0.03978	217.1	7.952
BAT99-55	WN11h	0.6481	0.03829	428.3	15.1
BAT99-85	WC4 (+OB)	-0.4681	0.03374	1197	37.19
BAT99-123	WO3	1.782	0.04259	150.7	5.909
BAT99-133	WN11h	0.3187	0.01856	580.1	9.914
R66	B0.5[e]	0.4201	0.01875	528.4	9.126
S35	B1[e] Iab	2.104	0.05634	112	5.806
R126	B0.5[e]	0.993	0.03794	311.7	10.89
R71	LBV	-0.9245	0.01292	1823	21.7
R127	LBV	-0.1097	0.03093	860.7	24.51